System-wide biochemical analysis reveals ozonide antimalarials initially act by disrupting *Plasmodium falciparum* haemoglobin digestion

Carlo Giannangelo[1#], Ghizal Siddiqui[1#], Amanda De Paoli[1], Bethany M. Anderson[2,3], Laura E. Edgington-Mitchell[2,3,4], Susan A. Charman[5] and Darren J. Creek[1]*

[1]Drug Delivery, Disposition and Dynamics, [2]Drug Discovery Biology, [5]Centre for Drug Candidate Optimisation, Monash Institute of Pharmaceutical Sciences, Monash University, Parkville Campus, Parkville, Victoria Australia.

[3]Department of Biochemistry and Molecular Biology, Bio21 Molecular Science and Biotechnology Institute, The University of Melbourne, Melbourne, Victoria, Australia.

[4]Department of Maxillofacial Surgery, College of Dentistry, New York University, New York, New York, USA.

[#] These authors contributed equally

* To whom correspondence should be addressed to Dr. Darren Creek, Drug Delivery, Disposition and Dynamics, Monash Institute of Pharmaceutical Sciences, Monash University, Parkville Campus, Parkville, Victoria, Australia. Tel: +61 (0) 3 9903 9249; Fax: +61 (0) 3 9903 9583; e-mail, Darren.creek@monash.edu

Abstract

Ozonide antimalarials, OZ277 (arterolane) and OZ439 (artefenomel), are synthetic peroxide-based antimalarials with potent activity against the deadliest malaria parasite, *Plasmodium falciparum*. Here we used a "multi-omics" workflow, in combination with activity-based protein profiling (ABPP), to demonstrate that peroxide antimalarials initially target the haemoglobin (Hb) digestion pathway to kill malaria parasites.

Time-dependent metabolomic profiling of ozonide-treated *P. falciparum* infected red blood cells revealed a rapid depletion of short Hb-derived peptides followed by subsequent alterations in lipid and nucleotide metabolism, while untargeted peptidomics showed accumulation of longer Hb-derived peptides. Quantitative proteomics and ABPP assays demonstrated that Hb-digesting proteases were increased in abundance and activity following treatment, respectively. The association between ozonide activity and Hb catabolism was also confirmed in a *K13*-mutant artemisinin resistant parasite line. To demonstrate that compromised Hb catabolism may be a primary mechanism involved in ozonide antimalarial activity, we showed that parasites forced to rely solely on Hb digestion for amino acids became hypersensitive to short ozonide exposures.

Quantitative proteomics analysis also revealed parasite proteins involved in translation and the ubiquitin-proteasome system were enriched following drug treatment, suggestive of the parasite engaging a stress response to mitigate ozonide-induced damage. Taken together, these data point to a mechanism of action involving initial impairment of Hb catabolism, and indicate that the parasite regulates protein turnover to manage ozonide-induced damage.

Author Summary

The ozonides are a novel class of fully synthetic antimalarial drugs with potent activity against all parasite species that cause malaria, including the deadliest, *Plasmodium falciparum*. With the emergence of resistance to current frontline artemisinin-based antimalarials, new drugs are urgently needed and a clear understanding of their mechanism of action is essential so that they can be optimally deployed in the field. Here, we studied the biochemical effects of two ozonides, OZ277 (marketed in India in combination with piperaquine) and OZ439 (in Phase IIb clinical trials) in *P. falciparum* parasites using an untargeted multi-omics approach consisting of proteomics, peptidomics and time-dependent metabolomics, along with activity-based protease profiling. We found that the ozonides initially disrupt haemoglobin metabolism and that they likely engage the parasite proteostatic stress response. Furthermore, when the duration of ozonide exposure was extended beyond 3 hours to reflect clinically-relevant exposure periods, additional parasite biochemical pathways were perturbed. This comprehensive analysis provides new insight into the antimalarial mode of action of ozonides and provides new opportunities for interventions to enhance their antimalarial efficacy.

Introduction

Promising improvements in malaria control have been recorded over the last two decades, but recent data indicates that the declining mortality rates have either stalled or increased in many malaria endemic regions since 2016 [1]. The absence of a reliable and highly efficacious vaccine means that treatment is heavily reliant on effective antimalarial chemotherapy. Currently, the World Health Organisation (WHO) recommends artemisinin-based combination therapies (ACTs) as the first-line treatment for uncomplicated *Plasmodium falciparum* malaria in all endemic areas [2]. The artemisinins (including dihydroartemisinin, DHA) contain an essential peroxide bond that undergoes reductive activation by haem released through parasite haemoglobin (Hb) digestion [3-6]. This activation process generates highly reactive drug-derived radicals that mediate rapid parasite killing [7]. However, artemisinins are limited by poor biopharmaceutical properties and short *in vivo* half-lives (< 1 h) [7-9]. Furthermore, the emergence of artemisinin resistant parasites now threatens global malaria control and elimination efforts [10]. Thus, there is a desperate need for improved therapeutics to combat malaria.

To overcome some of these limitations, the artemisinin peroxide bond inspired the design of fully synthetic and structurally dissimilar peroxide-based antimalarials, known as ozonides [11] (Fig. 1). The first-generation ozonide, OZ277 (later known as RBx11160 or arterolane) [11], was the first to be approved clinically and is currently marketed as a fixed dose combination with piperaquine (Synriam^{TM}). However, the *in vivo* half-life of OZ277 is only 2- to 3-fold longer than that for DHA [12, 13]. This rapid clearance is thought to be associated with both hepatic metabolism [14] and instability of the peroxide bond when exposed to endogenous sources of iron in blood and tissues [15]. A design strategy aimed at stabilising the peroxide bond to iron-mediated degradation led to the development and selection of the second-generation ozonide, OZ439 (artefenomel) [15]. When tested clinically, OZ439 exhibited an *in*

vivo half-life of 46-62 h in humans [16, 17]. OZ439 is currently in Phase IIb clinical trials in combination with ferroquine (ClinicalTrials.gov Identifier: NCT02497612).

Ozonide antimalarials display similar clinical efficacy to DHA, rapidly clearing blood-stage parasites [17, 18]. However, their antimalarial mechanism of action (MoA) has been less extensively studied than the artemisinins, and debate remains about the key molecular events responsible for artemisinin action [19-24]. The current model for ozonide antimalarial activity is that Hb-derived free haem mediates reductive activation of the peroxide bond giving rise to toxic carbon-centred radicals [25] that alkylate a number of essential parasite proteins from various biochemical pathways [26, 27]. Crucially, optimal clinical utilisation of ozonides will rely on a clear understanding of the biochemical mechanisms that underpin their activity. Therefore, we investigated the temporal biochemical response of *P. falciparum* parasites treated with OZ277 and OZ439 using systems-wide analyses, incorporating time-dependent metabolomics and proteomics. We identified Hb digestion as the key initial pathway targeted by ozonide antimalarials and demonstrated that when parasites are forced to rely solely on Hb digestion for nutrients, they become hypersensitive to pulsed ozonide treatment. Furthermore, we showed that ozonides perturb additional pathways when treatment was extended beyond 3 h, reflecting more clinically-relevant exposures for the ozonides, and that parasites likely regulate protein turnover to manage ozonide-mediated damage. This work provides new opportunities for interventions to target malaria parasites and enhance ozonide antimalarial efficacy.

Results

Ozonide antimalarials initially deplete short haemoglobin (Hb)-derived peptides

In order to distinguish the early peroxide-induced effects from secondary mechanisms, we employed a time-dependent, untargeted metabolomics approach that allowed comprehensive biochemical profiling of the primary pathways affected by ozonide antimalarials in *P. falciparum* infected red blood cells (iRBCs) (Supplementary Fig. 1). Trophozoite-stage parasites (28-34 h post invasion) were treated with 300 nM of OZ277 or OZ439 or 100 nM of DHA over a time course of up to 3 h (n = at least four biological replicates). These drug concentrations are equivalent to the IC_{50} for a 3 h pulse, under the same *in vitro* conditions used in the metabolomics analysis (10% parasitaemia and 2% Hct) [28], and are within therapeutic concentration ranges [10, 17, 29]. Univariate analysis of the untargeted metabolomics dataset (Supplementary Dataset 1) revealed a temporal increase in the percentage of drug-induced metabolic changes (Supplementary Fig. 2a) and that widespread metabolic perturbations were not evident after short drug exposures (Supplementary Fig. 2b). The ozonides rapidly and disproportionately affected peptide metabolism, with approximately 15-25% of all putatively identified short peptides (2-4 amino acids in length) significantly perturbed within 3 h of drug treatment (P-value < 0.05) (Supplementary Fig. 2b). These significantly perturbed peptides were parasite-specific metabolites (Supplementary Dataset 1) and exhibited a progressive depletion in abundance over the 3 h drug exposure (Fig. 2a and 2b). Interestingly, the extent of peptide depletion was more extensive and faster in DHA-treated parasites compared to the ozonides, which is consistent with the more rapid kinetics of antiparasitic activity previously observed for DHA compared to the ozonides for these short pulse exposures (< 3 h) [30]. The amino acid sequence of a subset of these putatively identified peptides was confirmed by MS/MS and the majority of perturbed peptides (i.e., those that were decreased by at least 1.5-fold) could be mapped to either the alpha or beta chains of Hb (Fig. 3a).

A similar, although less extensive, temporal increase in the number of significant metabolic perturbations was confirmed in ring-stage parasites (6-12 h post invasion) treated with ozonide antimalarials (Supplementary Fig. 3a), with putative Hb-derived peptides representing the first metabolites to be significantly perturbed (Supplementary Dataset 1 and Supplementary Fig. 3b). This was further verified using multivariate analysis, where sparse partial least squares–discriminant analysis (sPLS-DA) revealed that Hb-derived short peptides were responsible for the greatest differences between the ozonide-treated samples and controls (Supplementary Fig. 4). Similar to trophozoite-stage parasites, these Hb peptides showed a time-dependent depletion in the treated parasite cultures compared to controls (Fig. 3c).

To further investigate the importance of parasite Hb digestion to ozonide antimalarial action, untargeted metabolomic profiling was also performed on artemisinin resistant (Cam3.II^{R539T}) and isogenic sensitive (Cam3.II^{rev}) [31] early trophozoite-stage (22-26 h post invasion) parasites (Supplementary Dataset 2). Artemisinin resistant early trophozoite-stage parasites have been shown to exhibit differential sensitivity to short DHA exposures compared to the isogenic sensitive strain, albeit a less dramatic difference than early rings [32]. Targeted analysis of the LC-MS raw data identified 26 perturbed peptides (at least 1.5-fold) in drug-treated resistant (Cam3.II^{R539T}) or sensitive parasites compared to control (Fig. 2d). The majority (> 70%) of perturbed peptides were depleted in treated samples compared to the control (Fig. 2d and Supplementary Fig. 5a) and most of these peptides (all except two) could be mapped to Hb (Supplementary Fig. 5b). Notably, the extent of peptide depletion was greater in the sensitive parasites than in the resistant line (Fig. 2d). In general, the abundance of these peptides in treated resistant parasites remained at, or above, the basal levels detected in untreated sensitive parasites.

Ozonide antimalarial treatment causes accumulation of long chain Hb peptides

The rapid depletion of short chain Hb-derived peptides led us to consider how ozonide antimalarial exposure impacts longer Hb-derived peptides. We used a MS/MS-based global peptidomics approach (Supplementary Fig. 1) to examine the abundance of endogenous peptides (< 10 kDa) within ozonide-treated *P. falciparum* parasites. Peptidomics analysis identified a total of 59 endogenous *P. falciparum* peptides and 59 endogenous human peptides (Supplementary Dataset 3). OZ277 (300 nM for 3 h) treatment significantly altered the abundance of 30 endogenous peptides in trophozoites-stage parasites (P-value < 0.05), 17 of which originated from Hb (alpha and beta), and were increased in abundance (Fig. 3b). A similar build-up of long chain Hb peptides was also observed following treatment with OZ439 (300 nM for 3 h). Unlike the ozonides, exposure of trophozoite-stage parasites to 3 h of DHA (100 nM) predominantly depleted the abundance of Hb-derived peptides, with 26 peptides significantly depleted and four significantly elevated relative to control (Fig. 3b). The differential impact of ozonides and DHA on longer chain Hb-derived peptides may be explained by the faster onset of action of artemisinins compared to ozonides [30]. Indeed, a shorter DHA exposure (1 h) caused an accumulation of longer Hb peptides similar to the ozonides (Fig. 3c and Supplementary Dataset 4).

We also assessed whether the accumulated Hb components in peroxide-treated parasites differ from those in E64d (cysteine protease inhibitor)-treated parasites. E64d causes parasite digestive vacuoles to accumulate undegraded Hb and swell due to disruption of the initial endoproteolytic cleavage of Hb [33, 34]. Trophozoite-stage parasites treated with E64d for up to 3 h developed a characteristic swollen digestive vacuole (Supplementary Fig. 6a), consistent with abrogated digestion of full-length Hb. These same parasites exhibited a modest trend towards accumulation of intact Hb and minor changes in free haem and haemozoin levels (Supplementary Fig. 6a) when these haem-containing species were measured using haem fractionation assays [35]. Visualisation of monomer Hb (17 kDa) by Coomassie staining of

SDS-PAGE gels confirmed that undigested Hb accumulated in trophozoites after these short E64d exposures (Supplementary Fig. 6b). Conversely, peroxide-treated parasites showed a minor decrease in the levels of full-length Hb, when measured using the haem fractionation assay (no changes in other haem species were evident) (Supplementary Fig. 6a), which is broadly consistent with our quantitative proteomics data (Supplementary Fig. 6c). Peroxide exposures of up to 3 h caused no changes in digestive vacuole morphology, indicating that there is no inhibition of proteolysis of full-length Hb (Supplementary Fig. 6a). Taken together, these findings suggest that the accumulated Hb components in peroxide-treated parasites are likely different from those resulting from specific inhibition of cysteine proteases.

Our untargeted peptidomics analysis also showed that ozonide treatment perturbed the levels of some endogenous parasite peptides. Of the 13 parasite peptides significantly perturbed following OZ277 exposure, five originated from an uncharacterised *P. falciparum* protein (PF3D7_0716300) and were decreased in abundance compared to control (Supplementary Dataset 3). OZ439 treatment resulted in significant perturbations to five parasite peptides, four of which were from this same uncharacterised protein (PF3D7_0716300) and were decreased relative to the untreated (Supplementary Dataset 3). A total of 15 endogenous parasite peptides were altered in abundance following DHA treatment, including six peptides that originated from the uncharacterised protein PF3D7_0716300 and, similar to ozonide exposure, were significantly decreased compared to control (Supplementary Dataset 3).

Ozonide antimalarial treatment increases the abundance and activity of Hb proteases

Plasmodium parasites digest Hb through a semi-ordered proteolytic process incorporating numerous proteases of different classes [37]. Peptidomics and metabolomics analyses of treated parasites suggested that ozonide antimalarials disrupt Hb catabolism through inhibition of the proteases involved in the breakdown of large to small Hb peptides. In order to quantify

the abundance of the proteases involved in Hb digestion, we used dimethyl labelling-based quantitative proteomics (Supplementary Fig. 1) [38]. Targeted analysis of the global proteomics data (Supplementary Fig. 7 and Supplementary Dataset 5) identified falcipains 2 and 3 (FP 2 and FP 3) and the plasmepsins (PM I, PM II, PM IV and HAP), proteases thought to be involved in the initial stages of Hb degradation [37], to be elevated in abundance in drug-treated samples compared to control (Fig. 4a). Dipeptidyl aminopeptidase 1 (DPAP1), which removes dipeptides from the polypeptides produced by upstream proteases [39], and the alanyl aminopeptidase (*Pf*A-M1), leucyl aminopeptidase (*Pf*A-M17) and aspartyl aminopeptidase (*Pf*M18AAP) metalloproteases, all of which are involved in the terminal stages of Hb digestion [40], were all increased following ozonide treatment (Fig. 4a). No changes in the abundance of falcilysin (Fig. 4a) was detected (Supplementary Dataset 5).

As most Hb-degrading proteases were elevated in abundance after ozonide antimalarial treatment, we then investigated the temporal impact of ozonides on Hb protease activity using activity-based probes (ABPs) targeting parasite cysteine proteases [41] (Supplementary Fig. 1). Trophozoite-stage parasite cultures were treated with OZ277 or OZ439 (300 nM) for up to 5 h and the biotinylated epoxide ABP, DCG04 [42], was used to label the Hb-digesting cysteine proteases FP 2, FP 3 and DPAP1 in the parasite lysate under both acidic (pH 5.5) and neutral pH (pH 7.2) conditions. Both OZ277 and OZ439 caused a time-dependent increase in the activity of proteases with molecular weights consistent with that of the FPs (FP 2 and FP 3), and DPAP1 [43] (Fig. 4b). A similar increase in the activity of these proteases was observed under acidic (the pH environment of the parasite digestive vacuole) or neutral pH conditions (Supplementary Fig. 8a), and activity was inhibited by pre-treatment of the parasite lysate with the cysteine protease inhibitor, ALLN (Supplementary Fig. 8b). FPs and DPAP1 activity were increased within 1 h of OZ277 treatment compared with DMSO controls (Fig. 4b). In contrast, OZ439 increased FPs and DPAP1 activity after 3-5 h of drug exposure, consistent with it

having a slower onset of action within the parasite [30]. Ozonide-induced increases in activity of FPs and DPAP1 were further confirmed by another cysteine protease-targeting probe, FY01 [43], under both acidic (Supplementary Fig. 9a) and neutral (Supplementary Fig. 9b) conditions.

Impaired Hb digestion underpins initial ozonide-induced toxicity

Functional Hb uptake and digestion is essential for parasite survival as it supplies amino acids for protein synthesis [44]. As our multi-omics and ABPP analyses identified Hb catabolism as the primary pathway affected by ozonide antimalarial treatment, we hypothesised that drug-derived radicals initially target this pathway, disrupting Hb catabolism, and starving the parasite of Hb-derived amino acids. To test this, we determined the potency of peroxide antimalarials on parasites grown in full RPMI medium (with all 20 amino acids) (AA medium) and parasites cultured in medium lacking all exogenous amino acids except for isoleucine (the only amino acid absent from Hb) (Iso medium), thereby forcing parasites to rely solely on Hb catabolism for amino acid supply (Fig. 4c).

Similar to published results [44], parasites cultured in Iso medium had a minor growth defect of approximately 20% compared to parasites cultured in AA medium (Fig. 4d). Trophozoite-stage cultures exposed to OZ277 or OZ439 (both 300 nM) for 3 h were sensitised by 2.3- and 1.6-fold, respectively, in the Iso medium (Fig. 4e), suggesting that compromised Hb catabolism is the primary MoA of ozonides in the initial exposure phase. However, when drug pressure was maintained throughout the entire RBC life cycle, there was no difference in sensitivity between parasites cultured in the Iso and AA mediums (Supplementary Fig. 10), suggesting that mechanisms beyond disrupted Hb digestion contribute to parasiticidal activity during prolonged exposure. DHA treated parasites were almost 5-fold more sensitive in the Iso medium compared to parasites cultured in AA medium (Fig. 4e). In contrast, the potency of

pyrimethamine, which kills parasites by a mechanism independent of Hb digestion [45], was not affected when cultured in either AA or Iso medium (Fig. 4e).

Ozonide antimalarial treatment upregulates parasite proteasome and translation machinery proteins

Untargeted analysis of our global quantitative proteomics dataset (Supplementary Dataset 5 and Supplementary Fig. 7) identified that ozonide and DHA treatment causes a significant dysregulation of 24 to 281 proteins within 3 h of drug exposure. Clustering analysis of all proteins significantly (P-value ≤ 0.05 and fold-change ≥ 1.5) perturbed by OZ277 treatment revealed that translation regulation (P-value = $5.184E^{-7}$) and the proteasome system (P-value = $5.288E^{-4}$) were the two main pathways affected. Parasite proteins in these two networks were significantly enriched following OZ277 treatment (Fig. 5). Similar protein clustering was also observed for DHA (Supplementary Fig. 11) treatment, with elevated levels of proteins involved in translation regulation (P-value < $1.0E^{-9}$) and the proteasome system (P-value $3.691E^{-6}$). A trend towards increased abundance of translation regulation and proteasome system proteins was also observed following 3 h of OZ439 exposure (Supplementary Dataset 5), however no protein networks were significantly enriched.

Extended exposure disrupts secondary metabolic pathways involved in ozonide antimalarial activity

Using untargeted metabolomic profiling, we also investigated whether parasite biochemical pathways other than Hb metabolism were affected following long-term ozonide treatment (> 3 h). Extended exposure induced metabolic perturbations beyond peptide metabolism, including, amino acid, lipid, cofactor and vitamin, and nucleotide metabolism (Fig. 6a and Supplementary Dataset 1). It is possible that some of these secondary responses to prolonged drug treatment represent nonspecific responses from dying parasites, but it is noted that different drug-specific

responses were reported in similar metabolomics studies of other compounds [46-48], suggesting that these metabolic alterations are largely ozonide-specific. Extended treatment of trophozoite-stage parasites with OZ277 and OZ349 resulted in significant perturbations (P-value ≤ 0.05 and fold-change ≥ 1.5) to approximately 5% of the 217 putatively identified lipids (Supplementary Fig. 12). The major parasite neutral glycerolipid species, diglycerides (DG) and triglycerides (TG), were depleted within 6 h of ozonide exposure (Supplementary Fig. 12). DGs are the direct metabolic precursor of phosphatidylcholine (PC) and phosphatidylethanolamine (PE) lipids, the main glycerophospholipids in the parasite. Metabolites involved in PC and PE *de novo* synthesis accumulated in a time-dependent manner following extended ozonide treatment, while some of the PCs and PEs themselves, and other glycerophospholipids, were depleted (Fig. 6b and Supplementary Fig. 12). At the proteome level, four of the six enzymes in the *de novo* glycerophospholipid synthesis pathway (Kennedy pathway) were elevated after ozonide treatment compared to control (Fig. 6b and Supplementary Fig. 13). Prolonged treatment of rings (> 3 h) also disrupted *de novo* synthesis of PC and PE lipids (Supplementary Fig. 14).

Extended ozonide exposure also disrupted parasite pyrimidine nucleotide biosynthesis. Metabolites of the *de novo* pyrimidine biosynthesis pathway, L-aspartate, N-carbamoyl-L-aspartate and uridine monophosphate (UMP), were all depleted after drug treatment (Fig. 6c and Supplementary Fig. 15), while at the proteome level, four of the six enzymes in this pathway were elevated compared to the control (Fig. 6c and Supplementary Fig. 16).

Discussion

This study provides a detailed assessment of the *P. falciparum* biochemical pathways that are altered in response to ozonide antimalarial treatment. The "multi-omics" analysis revealed that ozonides act by rapidly perturbing parasite Hb catabolism prior to affecting other biochemical pathways, and suggested that the parasite regulates protein turnover to mitigate widespread ozonide-induced damage.

The time-resolved untargeted metabolomics approach allowed the mapping of primary and secondary ozonide-induced effects on parasite metabolism and revealed that short drug exposures induced rapid depletion of short-chain Hb-derived peptides, which was most pronounced in the more susceptible trophozoite-stage, in comparison to the less susceptible [28, 30] ring-stage parasites (Fig. 2 and Supplementary Fig. 3). It is noted that previous metabolomic profiling of ozonide-treated, magnetically purified *P. falciparum* cultures revealed no major alterations to parasite metabolism [48]. However, that was likely due to the high parasitaemia conditions (> 90%) of magnetically purified cultures inducing rapid ozonide degradation such that no measurable antimalarial activity could occur [28]. Consistent with previous reports [46, 47], our metabolomics analysis also showed that DHA induced depletion of short Hb-derived peptides. Interestingly, this occurred more rapidly for DHA than the ozonides (within 1.5 h of exposure versus 3 h of exposure), which agrees with the reported exposure time-dependence of activity for DHA and ozonides [30].

Digestion of host Hb is essential for parasite survival as it provides amino acids for parasite protein synthesis and has additional non-anabolic functions, such as maintaining osmotic stability of the iRBC [49-51]. Hb digestion is most active during the trophozoite-stage [52], resulting in extensive turnover of diverse Hb-derived peptides and the release of a high concentration of haem, which activates peroxide antimalarials within the parasite [3, 30, 53].

317 The extensive drug activation and Hb turnover in trophozoites likely explains the profound
318 impact of peroxide antimalarials on Hb-derived small peptides in trophozoites (in terms of both
319 the range of Hb peptides affected and magnitude of peptide depletion) compared to the ring-
320 stage (Fig. 2). Although it is generally assumed that little Hb digestion occurs within ring-stage
321 parasites, expression of active Hb-degrading proteases [30] and small haemozoin crystals (by-
322 products of Hb digestion) have been detected [54-56]. This indicates that a low level of active
323 Hb degradation occurs in ring-stage parasites and supports the observation of depleted Hb-
324 derived small peptides following ozonide treatment (Fig. 2c and Supplementary Fig. 3 and 4).

325 The accumulation of longer Hb-derived peptides (Fig. 3b) and depletion of shorter di, tri and
326 tetrapeptides (Fig. 2) suggests that the ozonides disrupt Hb catabolism through an inhibitory
327 effect on the proteases involved in the conversion of large to small Hb peptides. However, we
328 cannot rule out inhibition of the peptide transporters on the digestive vacuole membrane, or
329 general impairment of digestive vacuole function, as contributors to this peptide phenotype. In
330 response to perturbations within the digestive vacuole and impaired Hb catabolism, we propose
331 that the parasite increases the abundance and activity of all proteases involved in Hb digestion,
332 except falcilysin (Fig. 4a), which has been shown to localise to both the parasite apicoplast and
333 the digestive vacuole, suggesting that it may have a function beyond Hb catabolism [60, 61].
334 It is noted that the activity of cysteine proteases involved in Hb digestion was elevated within
335 1 h of ozonide exposure, before the first time point of significant small peptide depletion (1.5
336 h), suggesting that the rapid peroxide effect on Hb catabolism occurs before there is a detectable
337 change in small peptide levels using metabolomics.

338 Rapid disruption of Hb catabolism by the ozonides (and artemisinins) agrees with the
339 hypothesis that peroxide-based drugs are activated by Fe(II) or haem to produce reactive
340 intermediates in the parasite digestive vacuole where Hb digestion takes place. The resulting
341 ozonide-derived radicals were recently shown to alkylate haem within iRBCs after short drug

342 exposures [64] and the radicals may also alkylate and inactivate digestive vacuolar proteins,
343 including the proteases involved in Hb digestion [19, 20, 27]. Our findings suggest that the
344 digestive vacuole FPs are unlikely to be the Hb proteases initially targeted by the ozonides.
345 The activity of these enzymes increased after ozonide treatment (Fig. 4b) and cysteine protease
346 inhibition with E64d resulted in accumulation of full-length Hb and digestive vacuole swelling,
347 whereas these features were not seen in peroxide treated-parasites (Supplementary Fig. 6).
348 Ozonides (and artemisinins) are reported to alkylate proteins localised to the parasite digestive
349 vacuole, including proteases involved in Hb digestion, for example, plasmepsins [19, 20, 27],
350 which could be the initial intraparasitic protein targets of peroxide antimalarials. Consistent
351 with our hypothesis that disrupted Hb catabolism is the key early event initiated by peroxide
352 treatment, we demonstrated that the initial antiparasitic effects of peroxide exposure were
353 enhanced when parasites were forced to rely solely on Hb degradation for amino acids (Fig.
354 4e). Taken together, we propose that Hb digestion is the initial pathway affected as a result of
355 peroxide antimalarial treatment.

356 Depletion of short Hb-derived peptides following peroxide treatment was also confirmed in
357 artemisinin resistant and sensitive parasite lines (Fig. 2d) that exhibit differential sensitivity to
358 ozonides and DHA in short pulse assays [30, 31, 57]. The level of drug-induced peptide
359 depletion was generally less extensive in the *K13*-mutant (Cam3.II^{R539T}) compared to that in
360 the drug-treated *K13*-wildtype revertant strain (Cam3.II^{rev}) (Fig. 2d), suggesting that the
361 peroxide impact on Hb catabolism is diminished in resistant parasites. This diminished affect
362 may be a result of increased survival of *K13*-mutants following short peroxide exposure and
363 could be mediated by altered Hb metabolism [38, 65, 66], augmented antioxidant defence
364 pathways [38, 58, 59] or an enhanced stress response [32].

365 One caveat is that the precise origin of the depleted di, tri and tetrapeptides detected by
366 untargeted metabolomic screening cannot be definitively determined due to their short

sequences. MS/MS confirmation of the amino acid sequence was obtained for a subset of these depleted peptides and the confirmed sequences could be mapped to Hb. Furthermore, combined with additional lines of evidence pointing to a mechanism involving ozonide-induced disruption of Hb catabolism, it is likely that most of the small peptides that were perturbed by drug treatment originated from Hb. The short peptides unable to be mapped to Hb could originate from other RBC proteins or *Plasmodium* proteins, and could be associated with peroxide-induced inhibition of proteasome function and altered proteostasis [21]. It is important to note that the majority of peptides detected in the metabolome were not perturbed by drug treatment and most of these unaffected peptides could not be mapped to Hb. Furthermore, endogenous long peptides from only one *Plasmodium* protein were reproducibly perturbed by peroxide treatment. These data suggested that general parasite protein degradation was not significantly affected as a result of these short peroxide exposures.

Extended drug treatment (>3 h) induced disruption of additional biochemical pathways beyond Hb catabolism, including lipid and nucleotide metabolism (Fig. 6a), representing secondary biochemical pathways involved in peroxide activity. In both ring and trophozoite-stage parasites, drug treatment induced an accumulation of several metabolic intermediates in the *de novo* synthesis pathways of PC and PE lipids (known as the Kennedy Pathways) (Fig. 6b and Supplementary Fig. 12 and 14), which are the major lipid components of parasite membranes [46]. Proteomic analysis revealed that all enzymes directly upstream of the elevated metabolites in the Kennedy Pathways were also increased in abundance (Fig. 6b and Supplementary Fig. 13), possibly to increase the synthesis of PC and PE as a biochemical response to drug-induced membrane damage. These findings are consistent with the biological activity of ozonides and artemisinins involving non-specific damage to parasite membranes, such as the digestive vacuole and mitochondrial membranes [67, 68], through lipid peroxidation, which becomes apparent after an extended duration of drug exposure (> 3 h) and the production of reactive

oxygen species [67, 69-72]. Inhibiting the synthesis of key phospholipids is detrimental to parasite survival [73] and it is likely that perturbation to this pathway contributes to peroxide antimalarial activity.

Prolonged ozonide and DHA exposure in trophozoite-stage parasites also led to the depletion of DGs and TGs (Fig. 6b and Supplementary Fig. 12). These are the two main neutral glycerolipid species in parasites [74] and these lipids increase in abundance as the asexual parasite matures, indicating their importance for growth and development [74]. DGs and TGs are packaged into neutral lipid bodies, which are closely associated with the parasite digestive vacuole [75-77]. Neutral lipid bodies are thought to concentrate free haem and catalyse its biocrystallisation into non-toxic haemozoin [76-78], placing them proximal to the location where peroxide antimalarials are thought to be activated. Furthermore, fluorescently-tagged artemisinin and ozonide derivatives have been shown to accumulate in neutral lipid bodies [70, 71]. Activated drug, or potentially alkylated haem adducts [64], may therefore promote oxidative damage to DGs and TGs within neutral lipid bodies and limit the availability of key neutral lipids that are required for parasite development [74]. As DGs are key precursors for membrane phospholipid synthesis (e.g. PC and PE), it is expected that DG depletion also contributes to the upregulation of *de novo* phospholipid biosynthesis (Kennedy) pathways.

Disruption of the parasite pyrimidine biosynthetic pathway at both the metabolite and protein levels (Fig. 6c and Supplementary Fig. 15 and 16) was also apparent in ozonide and DHA treated parasites. This finding is consistent with previous studies demonstrating DHA-induced alterations in parasite pyrimidine metabolism [46]. Furthermore, carbamoyl phosphate synthetase and aspartate carbamoyl transferase, which catalyse the initial steps of parasite pyrimidine biosynthesis, are reported to be alkylation targets of artemisinins, although this has not yet been shown for the ozonides [19]. Peroxide-induced inhibition of one or both of these initial pyrimidine biosynthetic enzymes may be responsible for the depletion of downstream

417 pyrimidine biosynthesis intermediates, and a corresponding increase in the protein levels of
418 some enzymes in this pathway as a compensatory response, as shown in our study.

419 The alternative hypothesis that these secondary pathways are non-specific responses in dying
420 parasites is also possible. However, different drug-specific biochemical responses were
421 reported in metabolomics, proteomics and peptidomics studies of other antimalarials, even
422 when parasites were exposed to drugs for extended durations [46-48, 79, 80]. Combined with
423 reports showing that peroxide antimalarials target proteins in both the phospholipid and
424 pyrimidine biosynthesis pathways [19, 20, 27] and colocalise with neutral lipids within iRBCs
425 [70, 71], the drug-specific biochemical responses of parasites detected in metabolomics studies
426 suggests that the secondary metabolic alterations observed here are likely ozonide-specific and
427 related to the pleiotropic effect of peroxides on parasite metabolism.

428 Our work demonstrating that peroxide antimalarials affect multiple aspects of parasite
429 biochemistry is consistent with previous reports [46, 47]. Global proteomic analysis of ozonide
430 and DHA-treated parasites revealed a pronounced enrichment of proteins involved in protein
431 translation and the ubiquitin-proteasome system (Fig. 5 and Supplementary Fig. 11). Previous
432 studies have shown that artemisinins inhibit protein translation and proteasome activity [21,
433 81], and the observed enrichment in these pathways from our study may represent a response
434 to this inhibition, either by regulation of protein expression, or decreased degradation of these
435 proteins. Furthermore, the enrichment of proteins in the translation and proteasomal pathways
436 may reflect a general stress response to enhance protein turnover and mitigate peroxide-
437 mediated cellular damage [82]. Peroxide-induced oxidative insult and widespread protein
438 alkylation is thought to induce accumulation of damaged and misfolded proteins [22, 32, 83],
439 and the parasite relies on translational regulation and a functional ubiquitin-proteasome system
440 to restore proteostasis [84, 85].

Based on our findings, we have proposed a model for the MoA of peroxide antimalarials (Fig. 7). Hb-derived free haem activates the peroxide bond of ozonides (or artemisinins) within the digestive vacuole and the resulting drug-derived radicals initially alkylate haem [64] and damage proteases involved in Hb digestion leading to disruption of the Hb degradation pathway. In response to drug-induced damage, the parasite increases the abundance and activity of Hb-digesting proteases. Following prolonged exposure, drug-derived radicals induce further oxidative insult and cause widespread alkylation of parasite components, including damage to lipids, and proteins involved in other vital parasite functions. To mitigate drug-induced cellular damage, the parasite engages a proteostatic stress response involving upregulation of proteins involved in translational regulation and the ubiquitin-proteasome system. Parasite death ultimately occurs when drug-mediated damage overwhelms these parasite defensive mechanisms. In artemisinin resistance, *K13* mutations alter parasite Hb metabolism [38, 65, 66] and enhance antioxidant capacity [38, 58, 59] and stress response pathways [32], limiting the damage of drug-derived radicals and increasing parasite survival.

Although DHA had a more rapid and pronounced effect on metabolism compared to the ozonides, these antimalarials affected similar biochemical pathways suggesting that they have a similar MoA. This could raise concerns for the deployment of ozonides in areas affected by artemisinin resistance [86], which is characterised by infections with parasites that can withstand the short DHA exposures observed in the pharmacokinetics of clinically-used artemisinins [17, 30]. However, the temporal metabolomics analysis demonstrated that prolonged peroxide exposure perturbed additional pathways beyond the digestive vacuole, raising the possibility that long half-life ozonides (e.g. OZ439) may impact additional parasite functions during prolonged exposure, and potentially overcome resistance associated with the short-lived artemisinins. There are mixed reports regarding ozonide activity in artemisinin resistant parasites, and further clinical studies are required to determine the potential utility of

ozonides in artemisinin resistant malaria infections [64]. In the context of growing concerns about the spread of multi-drug resistant malaria parasites, this insight into the MoA of peroxide antimalarials, and the parasite's response to treatment, offers potential avenues for targeting the malaria parasite with novel drug regimens that have improved antimalarial efficacy and limit the generation of drug resistance.

Materials and Methods

Plasmodium falciparum culture conditions

P. falciparum parasites (3D7 strain, Cam3.II^{R539T}, and Cam3.II^{rev}) were cultured as previously described [87]. RBCs were obtained from the Australian Red Cross Blood Service in Melbourne. Artemisinin resistant and sensitive *P. falciparum* isolates were kindly provided by Professor David Fidock, Columbia University and included the field-derived *K13*-mutant, Cam3.II^{R539T}, and the *K13*-wildtype on an isogenic background (Cam3.II^{rev}) [31]. Parasites were tightly synchronised by double treatment with sorbitol [88]. For 3D7 parasites, trophozoite or ring stage parasite cultures were adjusted to 10% parasitaemia and 2% Hct. For experiments using artemisinin resistant and sensitive isolates, trophozoite parasite cultures were adjusted to 4% parasiteamia and 2% Hct.

Metabolomics sample preparation

In 3D7 parasites, comprehensive time-course analysis was performed to determine the peroxide-induced metabolic profile in ring- and trophozoite-stage parasites. Ring-stage parasite cultures (6-12 h post invasion) were exposed to drug (1 μM of OZ277 or OZ439, 300 nM of DHA and 0.03% DMSO) for 0, 3, 6 and 9 h prior to metabolite extraction, while trophozoite stage parasite cultures (28-34 h post invasion) were exposed to drug (300 nM of OZ277 or OZ439, 100 nM of DHA and < 0.03% DMSO) for 0, 0.5, 1.5, 3, 6 and 9 h.

In artemisinin resistant and sensitive isolates, prior to drug incubation, the age of paired artemisinin sensitive and resistant parasites was confirmed by analysis of Giemsa stained thin blood smears. Trophozoite parasite cultures (22-26 h) were exposed to 100 nM of DHA, OZ277 and OZ439 nM for a duration of 1, 3 and 5 h, respectively. Under the conditions used in this metabolomics study (4% parasitaemia and 2% Hct), these concentrations and exposure times were found to be sub-lethal in both the Cam3.II^{R539T} and Cam3.II^{rev} parasite lines (data not

shown). Metabolomics studies included treatment of non-infected RBCs as controls and all experiments were performed on at least three independent occasions.

Following drug incubation, for ring-stage experiments (3D7), metabolites were extracted from 2 x 10^8 cells using 200 µL of cold chloroform/methanol/water (1:3:1), while for trophozoite stage experiments (3D7), 1 x 10^8 cells were used and metabolites extracted using 150 µL of cold chloroform/methanol/water (1:3:1). For trophozoite stage experiments (3D7) where long-term peroxide treatment was used (up to 9 h), metabolites were extracted from 1 x 10^8 cells using 150 µL of cold methanol. For artemisinin resistant and sensitive isolates, 1 x 10^8 cells were used and metabolites extracted using 150 µL of cold methanol. Metabolomics extraction was as previously described [47]. Insoluble precipitates were removed by centrifugation and 110 µL of metabolite extract was transferred to glass LC-MS vials and stored at -80 °C until analysis. A 15 µL aliquot of each sample was combined to generate a pooled biological quality control (PBQC) sample for analytical quality control and metabolite identification procedures.

Metabolomics LC-MS analysis and data processing

Untargeted LC-MS analysis was performed using HILIC chromatography (ZIC-pHILIC; Merck®) with an alkaline mobile phase on an Ultimate U3000 LC system (Dionex) and Q Exactive Orbitrap MS (ThermoFisher®) operating in both positive and negative ion mode as previously described [38, 47]. The PBQC sample was run periodically throughout each LC-MS batch to monitor signal reproducibility and support downstream metabolite identification. Extraction solvent was used as blank samples to identify possible contaminating chemical species. To aid in metabolite identification, approximately 250 authentic metabolite standards were analysed prior to each LC-MS batch and their peaks and retention time manually checked using the ToxID software (Thermofisher®).

519 Metabolomics data were analysed using the IDEOM workflow [89]. High confidence
520 metabolite identification (MSI level 1) was made by matching accurate mass and retention time
521 to authentic metabolite standards [90]. Putative identifications (MSI level 2) for metabolites
522 lacking standards were based on exact mass and predicted retention times [91]. Specifically,
523 the identification of peptides was based on either accurate mass or a combination of accurate
524 mass and MS/MS analysis, which allowed definitive confirmation of the amino acid sequence
525 in selected peptides. In the ring and artemisinin resistance studies, LC-MS peak heights
526 representing metabolite abundances were normalised by median peak height, while quality
527 control procedures indicated that normalisation of metabolite abundances was not required in
528 the 3D7 trophozoite studies. Univariate statistical analysis was performed using IDEOM and
529 Welch's *t* test [89]. Multivariate statistical analysis was performed on the mean centred and
530 auto-scaled data using the web-based tools in Metaboanalyst [92]. Sparse partial least squares
531 – discriminant analysis (sPLS-DA) algorithms were run with increasing numbers of
532 metabolites in each component (up to 150 metabolites), with minor changes to the model when
533 more than 10 metabolites were used. The final sPLS-DA plots shown in the supplementary
534 data were developed using 10 metabolites in each component. Significant metabolites (P-value
535 ≤ 0.05) were confirmed by manual integration of raw LC-MS peak areas in TraceFinder™
536 (ThermoFisher®).

537 **Functional assays to measure haemoglobin abundance**

538 The Hb fractionation assay was adapted from [35, 80]. Briefly, 3D7 trophozoite-stage parasites
539 were incubated with DHA, OZ277, OZ439, E64d or a DMSO control for either 1 or 3 h.
540 Following incubation, Hb, haem and haemozoin species were separated and measured using
541 the Hb fractionation assay [35, 80], and smears were made using Giemsa stain to check for
542 parasite viability and digestive vacuole morphology by light microscopy. For the Hb
543 fractionation assay, the samples were normalised via a paired analysis to the DMSO control

and graphed as their fold change vs DMSO ± SD. All fractions had >4 replicates from >2 independent experiments.

Hb monomer was also measured using SDS-PAGE gel. Briefly, 3D7 trophozoite-stage parasites were incubated with OZ277, E64d or a DMSO control for 3 h. Following incubation, extracted parasites were resolved on SDS-PAGE gels and proteins stained using Coomassie blue.

Peptidomics sample preparation

Peptidomics samples were prepared as previously described with minor modifications [38]. Briefly, intracellular parasites were harvested after 3 h of drug treatment followed by trichloroacetic acid protein precipitation and centrifugal filtration using a 10 kDa cut-off filter (Amicon Ultra). The flow-through containing endogenous peptides was collected and peptide concentration was measured using a bicinchoninic acid (BCA) protein assay (Thermo Scientific Pierce) as per manufacturer's protocol. Equal concentration of peptides (53-75 µg) were used for peptidomic analysis. Peptide samples were then subjected to desalting using in-house generated C18 StageTips [93]. The elutes were then dried and resuspended in 20 µL of 2% (v/v) acetonitrile (ACN) and 0.1% (v/v) formic acid (FA) for LC-MS/MS analysis.

Peptidomics nanoLC-MS/MS analysis and data processing

LC-MS/MS analysis was performed using an Ultimate U3000 Nano LC system (Dionex) and Q Exactive Orbitrap MS (ThermoFisher®) as previously described [38].

Peptide identification was performed using PEAKS DB software [94]. Maximum mass deviation and false discovery rates were set at 0.5 Da and 0.01 respectively. No post translational modification or digestion were selected and identified peptide sequences were matched to *Homo sapiens* and *P. falciparum* databases. The mass to charge ratio and retention time of each identified peptide were imported into TraceFinder™ (ThermoFisher®) and the

peak intensity for each peptide was obtained manually. Further statistical analyses (Student's *t* test) were performed using Microsoft Excel for paired drug treated and DMSO control samples.

Proteomics sample preparation and triplex stable isotope dimethyl labelling

Proteomics samples were prepared as previously described with minor modifications [38]. Briefly, 1000 µg of protein, accurately determined using Pierce BCA assay, from each sample was incubated overnight with sequencing grade trypsin (Promega) (1:50) at 37℃. Quantitative triplex stable isotope dimethyl labelling was initiated on the following day using light, intermediate or heavy dimethyl labelling reagents [95]. The samples were then subjected to ion-exchange fractionation using a disposable Strong Cationic Exchange Solid Phase Extraction cartridge (Agilent Bond Elut) [96]. The fractions were desalted using in-house generated StageTips [93], dried and resuspended in 20 µL of 2% (v/v) ACN and 0.1% (v/v) FA for LC-MS/MS analysis.

Proteomics nanoLC-MS/MS analysis and data processing

LC-MS/MS analysis was performed using an Ultimate U3000 Nano LC system (Dionex) and Q Exactive Orbitrap MS (ThermoFisher®) as previously described [38]. Protein identification and quantification was performed using the MaxQuant proteomics software [97]. The data analysis parameters in MaxQuant were set as previously described [38] with minor modifications. Dimethylation settings were adjusted to triplets; DimetNterm0 with DimetLys0, DimetNterm4 with DimetLys4 and DimetNterm8 with DimetLys8 were selected as light, intermediate and heavy label respectively. To correct for differences in protein amount between groups, the protein ratios were normalised in MaxQuant at the peptide level so that the log2 ratio is zero [97]. Known contaminants such as trypsin, keratin and reverse sequences were removed from the MaxQuant output. Fold-changes for the drug treated samples relative to the DMSO control samples were calculated in Microsoft Excel. One sample t-test was used to test

the mean of combined experiment groups against the known mean ($\mu = 0$) [98]. For each drug, the proteins that were identified in at least three independent experiments were filtered based on P-value (≤ 0.05) and fold-change (≥ 1.5) to generate a list of significantly perturbed proteins. The bioinformatics interaction network analysis tool STRINGdb [99] was used to build a protein-protein interaction network using the significantly perturbed proteins. Connectivity was based on experimental, database and co-expression evidence and a strict minimum interaction score (> 0.7) was applied to limit false positive associations in the predicted network. The STRINGdb protein connectivity output was exported to Cytoscape 3.6[100] and the ClusterONE algorithm was used to integrate and visualise relationships between proteins that were significantly perturbed by drug treatment.

Temporal activity-based protein profiling of cysteine protease activity using activity-based probes

Activity-based probes (ABPs) were used to measure protease activity [43] following ozonide exposure according to established methods [101]. In these assays, tightly synchronised trophozoite stage parasites (28-34 h post invasion, 10% parasitaemia and 2% Hct) were treated with OZ277 (300 or 1000 nM) or OZ439 (300 nM) for up to 5 h. Untreated parasite controls contained an equivalent volume of DMSO ($< 0.01\%$). Following ozonide treatment, parasites were purified by lysing the red blood cells using 0.1% saponin on ice. Parasite pellets were then lysed by sonication in citrate buffer (50 mM trisodium citrate [pH 5.5], 0.5% CHAPS, 0.1% Triton X-100, 4 mM dithiothreitol) or phosphate buffered saline (PBS) (pH 7.2). Supernatants were then cleared by centrifugation and transferred to new tubes. Protein concentration in each sample was determined using BCA protein assay (Pierce) and an equal amount of each sample was incubated with ABPs (DCG04; 2 µM or FY01; 1 µM) for 30 min at 37 °C to label active cysteine proteases. In experiments including the reversible cysteine protease inhibitor N-acetyl-Leu-Leu-Norleu-al (ALLN) (Merck), parasite lysates were pre-incubated with 10 µM

of the inhibitor for 30 min prior to addition of the ABP for a further 15 min. In all cases, the reaction was quenched by the addition of 5x reducing buffer (50% glycerol, 250 mM Tris-Cl [pH 6.9], 10% SDS, 0.05% bromophenol blue, 6.25% beta-mercaptoethanol), boiled and separated by sodium dodecyl sulfate polyacrylamide (SDS-PAGE) on 15% polyacrylamide gels. As DCG04 is biotin-tagged, proteins were transferred to nitrocellulose membranes and incubated with streptavidin-AlexaFluor-647 followed by fluorescence detection with a Cy5 filter (excitation/emission: 649/670 nm) with an Amersham Typhoon 5 Biomolecular Imager (GE Healthcare Life Sciences). FY01 contains a Cy5 fluorophore, thus visualization of its targets was achieved by direct scanning of the gel for Cy5 fluorescence. Coomassie staining was used to confirm equal protein loading. Images were processed and quantified in either ImageJ 1.51f or Adobe Photoshop Creative Cloud 2017.

Determination of antimalarial potency on parasites cultured in complete RPMI medium or medium lacking exogenous amino acids (except isoleucine)

Full RPMI medium 1640 (Sigma-Aldrich) contained all 20 amino acids and was supplemented with 5.94 g/l HEPES, 2.1 g/l $NaHCO_3$, 50 mg/l hypoxanthine and 5 g/l Albumax II (Lifetech), making AA medium. RPMI medium 1640 lacking all amino acids (Life Research) was supplemented with isoleucine (Sigma-Aldrich) at a final concentration of 147.5 µM to make Iso medium [44]. All other supplements (HEPES, $NaHCO_3$, hypoxanthine and Albumax II) were added as for AA medium above. To examine parasite susceptibility to the peroxide antimalarials in the Iso and AA mediums, drug pulse activity assays were performed as previously described [102]. Briefly, the medium of iRBC cultures containing 30 h trophozoite-stage parasites (10% parasitaemia and 2% Hct) was replaced with either Iso or AA medium immediately before initiating drug treatment. Parasites were treated with 300 nM of pyrimethamine, OZ277 or OZ439 or 100 nM of DHA for 3 h. Following the incubation period, drugs were removed by washing the cultures as previously described [28] using either AA or

Iso medium supplemented with 2-5% Albumax II. Cultures were then adjusted to 0.5% parasitaemia and 2% Hct (final volume, 200 µL) as previously described [28] with either Iso or AA medium. After 48 h the parasitaemia was measured by counting Giemsa stained thin blood smears. Parasite survival was determined by graphing the parasitaemia for each test compound relative to the appropriate untreated medium (Iso or AA) control, which was set to 100%. All assays were performed in triplicate in at least three independent experiments.

Data availability

Proteomics and Peptidomics mass spectrometry data and search results have been deposited to the ProteomeXchange Consortium via the PRIDE [103] partner repository with the dataset identifier PXD014313 and project name 'System-wide biochemical analysis reveals ozonide and artemisinin antimalarials initially act by disrupting malaria parasite haemoglobin digestion'. Reviewers can access the dataset by using the username 'reviewer93735@ebi.ac.uk' and password 'RQivOi19'.

Metabolomics spectrometry data is available at the NIH Common Fund's Metabolomics Data Repository and Coordinating Center website, the Metabolomics Workbench http://metabolomicsworkbench.org, where it has been assigned Project ID PR000809. The data can be accessed directly via its project DOI: 10.21228/M83X38.

Acknowledgments

The authors thank Professor Matthew Bogyo (Stanford University School of Medicine) and Doctor Edgar Deu (The Francis Crick Institute) for providing the FY01 probe. Doctor Edgar Deu is also gratefully acknowledged for advice regarding activity-based protein profiling experiments. The authors thank Professor David Fidock (Columbia University) for provision of the genetically modified Cam3.II^{R539T} and Cam3.II^{rev} *P. falciparum* isolates. The Monash Proteomics and Metabolomics Facility (Parkville Node) provided technical assistance with metabolomics and proteomics experiments. The Australian Red Cross Blood Service in

667 Melbourne donated human red blood cells for *in vitro* parasite cultivation. Funding support
668 was provided by the Australian National Health and Medical Research Council (NHMRC)
669 project grants #APP1128003 and #APP1160705 and fellowship to D.J.C. (#APP1148700).
670 L.E.-M is funded by an Australian Research Council (ARC) Discovery Early Career
671 Researcher Award (DECRA) Fellowship (DE180100418) and the Grimwade
672 Fellowship funded by the Russell and Mab Grimwade Miegunyah Fund at the University of
673 Melbourne.

674 **Author contributions**

675 C.G., G.S., S.A.C., and D.J.C. designed the experiments. C.G., G.S., A.D.P., and B.M.A
676 executed the experiments. C.G., and G.S performed the mass spectrometry experiments. C.G.,
677 and G.S. analysed the data. C.G., G.S., L.E.-M., S.A.C., and D.J.C. wrote the manuscript. D.J.C
678 supervised the study.

679 **Competing interests**

680 The authors declare no competing interests.

681

683 **Figure legends**

684 **Fig. 1 Chemical structures of selected peroxide antimalarials.** The fully synthetic ozonide
685 antimalarials, OZ277 (arterolane) and OZ439 (artefenomel), and the clinically used
686 semisynthetic artemisinin derivative, dihydroartemisinin (DHA).

687 **Fig.2 Peroxide-induced perturbations to peptide metabolism. a**, Heatmap showing the
688 average fold change for all identified peptides at each time point after treatment with OZ277,
689 OZ439 and DHA. Values represent the average of at least three biological replicates, expressed
690 relative to the average untreated control value (at least seven biological replicates) for that
691 respective time point. **b**, Representative time profiles showing the progressive depletion in
692 abundance of selected putative haemoglobin-derived peptides after peroxide treatment of
693 trophozoite-stage parasites. Values are the average fold change (± SD) relative to the untreated
694 control of at least three biological replicates. **c**, Time-dependent decrease in the abundance of
695 the four peptides consistently depleted following peroxide treatment in ring infected cultures.
696 Values are the average fold change (± SD) relative to the untreated control of four biological
697 replicates. **d**, Heatmap of the peptides that were altered in abundance (≥ 1.5-fold relative to the
698 untreated control) following peroxide treatment in the *K13*-wildtype artemisinin sensitive
699 (Cam3.II^{rev}) and *K13*-mutant artemisinin resistant (Cam3.II^{R539T}) parasite lines. Data shown
700 are the average for three or five biological replicates expressed relative to the average for the
701 untreated control from the same parasite line.

702 **Fig. 3 Sequence coverage and relative abundance of haemoglobin alpha (Hb α) and**
703 **haemoglobin beta (Hb β) peptides detected after peroxide treatment. a**, Sequence coverage
704 for putative Hb-derived di-, tri-, and tetra-peptides that were differentially abundant (≥ 1.5-fold)
705 following peroxide antimalarial treatment relative to the untreated control (3D7 parasites). The
706 peptide sequences PA, PT, PE, PEE, HLD, SLD, PPVQ, PVNF and HVDD have been
707 confirmed by MS/MS analysis. For all other putative peptide sequences, all potential isomers

have been mapped. **b**, Sequence coverage for all long Hb α and Hb β peptides detected in peptidomics studies. Peptide abundances are the average fold change following 3 hours of drug treatment (OZ277, OZ439 and DHA), expressed relative to the untreated control (DMSO) from at least three biological replicates (3D7 parasites). **c**, Sequence coverage for Hb α and Hb β peptides detected following 1 hour of DHA treatment in Cam3.II^{rev} (artemisinin sensitive) parasites. Peptide abundances are the average fold change expressed relative to the untreated control (DMSO) from two biological replicates. In **b**, **c**, samples were normalised according to peptide concentration (measured using a bicinchoninic acid assay) during sample preparation. The solid lines represent the amino acid sequences of peptides that significantly changed in abundance after drug treatment relative to the untreated control (P-value < 0.05). Dashed lines represent non-significant (NS) changes. Increased and decreased peptide abundance are represented by red and blue (solid or dashed) lines, respectively.

Fig. 4 Peroxide antimalarials act by perturbing haemoglobin digestion. a, Disruption of protease abundance in the haemoglobin digestion pathway [37]. Values are the average $\log_2$ fold change (± SD) relative to the untreated control of at least three biological replicates. Trophozoite infected cultures were incubated with OZ277, OZ439 (both 300 nM) or DHA (100 nM) for 3 h. Falcipain 2 (FP 2) was identified in only two OZ277 treatment experiments, therefore the mean alone is shown. Aminopeptidase P (*Pf*APP) was not identified in any of the proteomic experiments. DPAP1, dipeptidyl aminopeptidase 1; FP, falcipain; HAP, histo-aspartic protease; *Pf*APP, aminopeptidase P; *Pf*A-M1, alanyl aminopeptidase; *Pf*A-M17, leucyl aminopeptidase; *Pf*M18APP, aspartyl aminopeptidase; PM, plasmepsin; * P-value < 0.05. **b**, Parasite cysteine protease activity after peroxide treatment using the activity-based probe (ABP), DCG04. Cysteine protease activity and densitometric analysis of the falcipain (FP) 2/3 and dipeptidyl aminopeptidase 1 (DPAP1) signal after OZ277 and OZ439 treatment in *P. falciparum* trophozoite stage parasites using DCG04 in lysates at pH 5.5 (acidic). Trophozoite

infected cultures were incubated with OZ277, OZ439 (both 300 nM) or an equivalent volume of DMSO (control). DCG04 labelling was detected by blotting membranes with streptavidin-AF647 after SDS-PAGE and transfer. The lanes for each time point are independent drug treatments and represent at least three biological replicates per time point that were run on the same gel side-by-side. For the densitometric analysis, the post drug treatment FP 2/3 and DPAP1 signal intensity was normalised to the average signal intensity of the appropriate time point in the untreated control (±SD). **c**, Schematic showing that infected RBCs treated with DHA or ozonides (OZ) can use exogenous amino acids when cultured in AA medium (Full RPMI medium with all 20 amino acids) in response to disrupted haemoglobin digestion (arrow shown in blue), while parasites in Iso medium (supplemented with isoleucine alone at a final concentration of 147.5 μM) must rely solely on haemoglobin digestion for amino acids. **d**, Amino acid requirement for cultured *P. falciparum* 3D7 parasites. Parasite viability measured following 48 h incubation in medium containing all amino acids (AA, black bars) and isoleucine alone medium (Iso, grey bars). **e**, Parasite sensitivity to peroxides when cultured in AA (black bars) medium compared to Iso (grey bars) medium. Trophozoite infected cultures were incubated with pyrimethamine, OZ277, OZ439 (all 300 nM), DHA (100 nM) or an equivalent volume of DMSO (control) for 3 h. Data represents the mean ± SD of at least three biological replicates. Growth values for each treatment is expressed relative to the appropriate untreated medium (Iso or AA) control, which was set to 100%. * P-value < 0.05.

Fig. 5 OZ277-induced disruption to the *P. falciparum* proteome. Network analysis of trophozoite stage parasite proteins perturbed following treatment with OZ277 (300 nM for 3 h). The network analysis was built using the STRINGdb interaction network analysis output (connectivity was based on experimental, database and co-expression evidence with a minimum interaction score of 0.7) in Cytoscape 3.6 with the ClusterONE algorithm. Node size

represents P-value and node colour represents fold-change from at least three independent replicates.

Fig. 6 Peroxide-induced disruption of secondary biochemical pathways. a, Metabolic perturbations in trophozoite-stage parasite cultures. Pathway enrichment analysis showing the percentage of significantly perturbed metabolites (Welch's *t* test; P-value < 0.05 and fold change > 1.5) as a function of metabolite class for extended (3, 6 and 9 h) exposure with OZ277, OZ439 (both 300 nM) and DHA (100 nM). **b**, Peroxide-induced disruption of the phosphatidylcholine (PC) and phosphatidylethanolamine (PE) lipid biosynthesis pathways within *P. falciparum* parasites. The dashed arrows represent an alternative route for the synthesis of PC from ethanolamine (Etn) in *P. falciparum*. CCT, choline-phosphate cytidyltransferase; CDP-, cytidine-diphospho-; CEPT, choline/ethanolamine phosphotransferase; Cho, choline; CK, choline kinase; CMP, cytidine monophosphate; DAG/DG, diglyceride; DM-, dimethyl-; ECT, ethanolamine-phosphate cytidyltransferase; EK, ethanolamine kinase; Etn, ethanolamine; MM-, monomethyl; PC, phosphatidylcholine; PCho, choline phosphate; PE, phosphatidylethanolamine; PEtn, ethanolamine phosphate; PG, phosphatidylglycerol; PMT, phosphoethanolamine N-methyltransferase; PS, phosphatidylserine; PSD, phosphatidylserine decarboxylase; PSS, phosphatidylserine synthase; SD, serine decarboxylase. **c**, Peroxide-induced perturbation of pyrimidine biosynthesis in trophozoite-stage parasite cultures. Hb, haemoglobin; UMP, uridine monophosphate. In **b**, **c**, metabolites (circles) and proteins (squares) in red and blue were increased and decreased in abundance after drug treatment, respectively. Yellow and black represent no change and not detected, respectively.

Fig. 7 Proposed model for ozonide antimalarial activity in *P. falciparum* infected red blood cells. Haemoglobin-derived haem activates peroxide antimalarials within the parasite digestive vacuole. The resulting drug-derived radicals initially damage components proximal

to the activation site, including proteases involved in haemoglobin digestion (arrow shown in blue). This leads to disruption of the haemoglobin degradation pathway. To correct for peroxide-induced damage, parasites may respond by increasing the abundance and activity of proteases involved in haemoglobin catabolism. Peroxide radicals induce further oxidative insult and cause widespread alkylation of parasite components as the duration of drug exposure is increased (arrows shown in green). This may include damage to lipids, inducing upregulation of the Kennedy Pathways, and proteins involved in other vital parasite functions, such as pyrimidine biosynthesis. To mitigate peroxide-induced cellular damage, the parasite engages a stress response involving translational regulation and the ubiquitin-proteasome systems. Asp, aspartic acid; ATC, aspartate carbamoyltransferase; C-Asp, carbamoyl-aspartate, C-Phos, carbamoyl-phosphate; CCT, choline-phosphate cytidyltransferase; CDP-, cytidine-diphospho-; CEPT, choline/ethanolamine phosphotransferase; Cho, choline; CK, choline kinase; CMP, cytidine monophosphate; CPS, carbamoyl phosphate synthetase; DHO, dihydroorotate; DHODH, dihydroorotate dehydrogenase; DHOtase, dihydroorotase; DV, digestive vacuole; ECT, ethanolamine-phosphate cytidyltransferase; EK, ethanolamine kinase; Etn, ethanolamine; Gln, glutamine; Hb, haemoglobin; OMPDC, orotodine 5'-phosphate decarboxylase; OPRT, orotate phosphoribosyltransferase; PC, phosphatidylcholine; PE, phosphatidylethanolamine; PCho, choline phosphate; PEtn, ethanolamine phosphate; PMT, phosphoethanolamine N-methyltransferase; RBC, red blood cell; UMP, uridine monophosphate.

803 **Fig. 1**

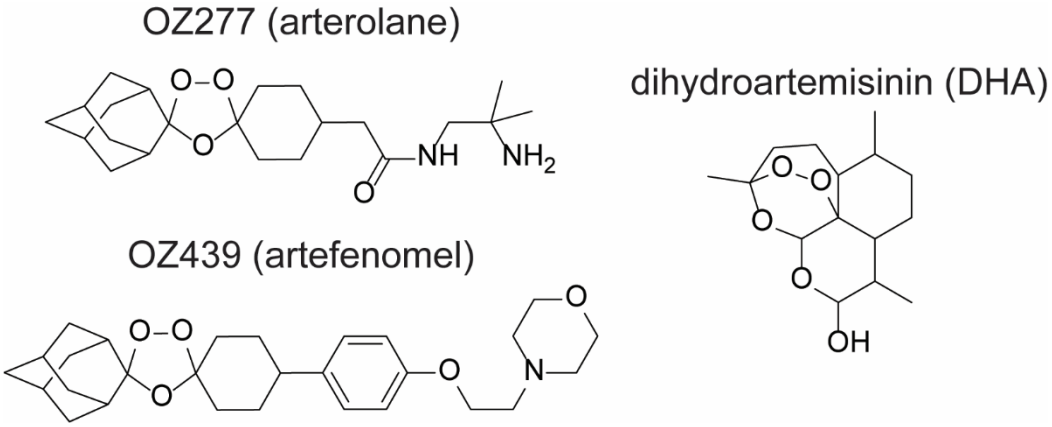

804

805

806 **Fig. 2**

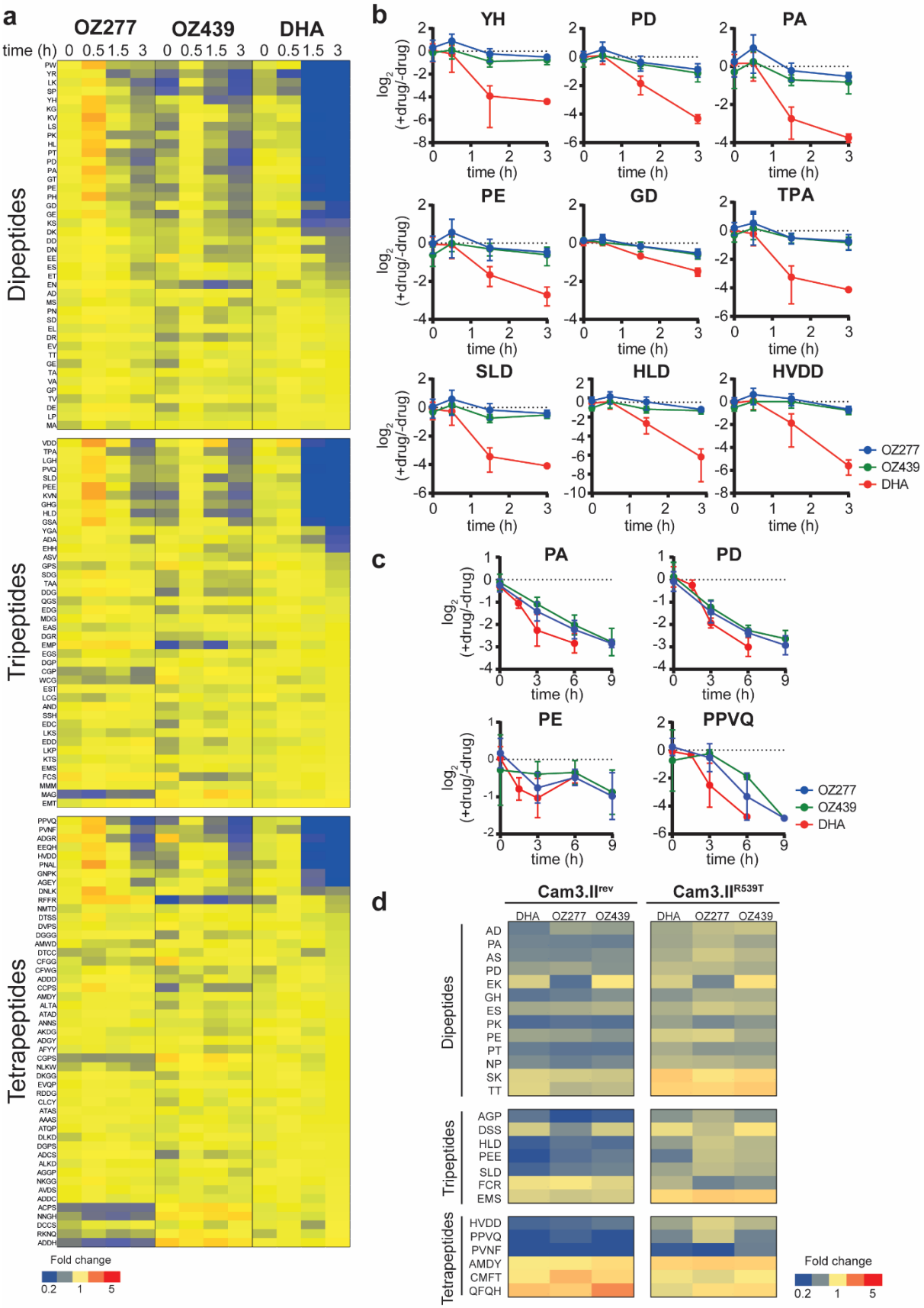

807
808

809 **Fig. 3**

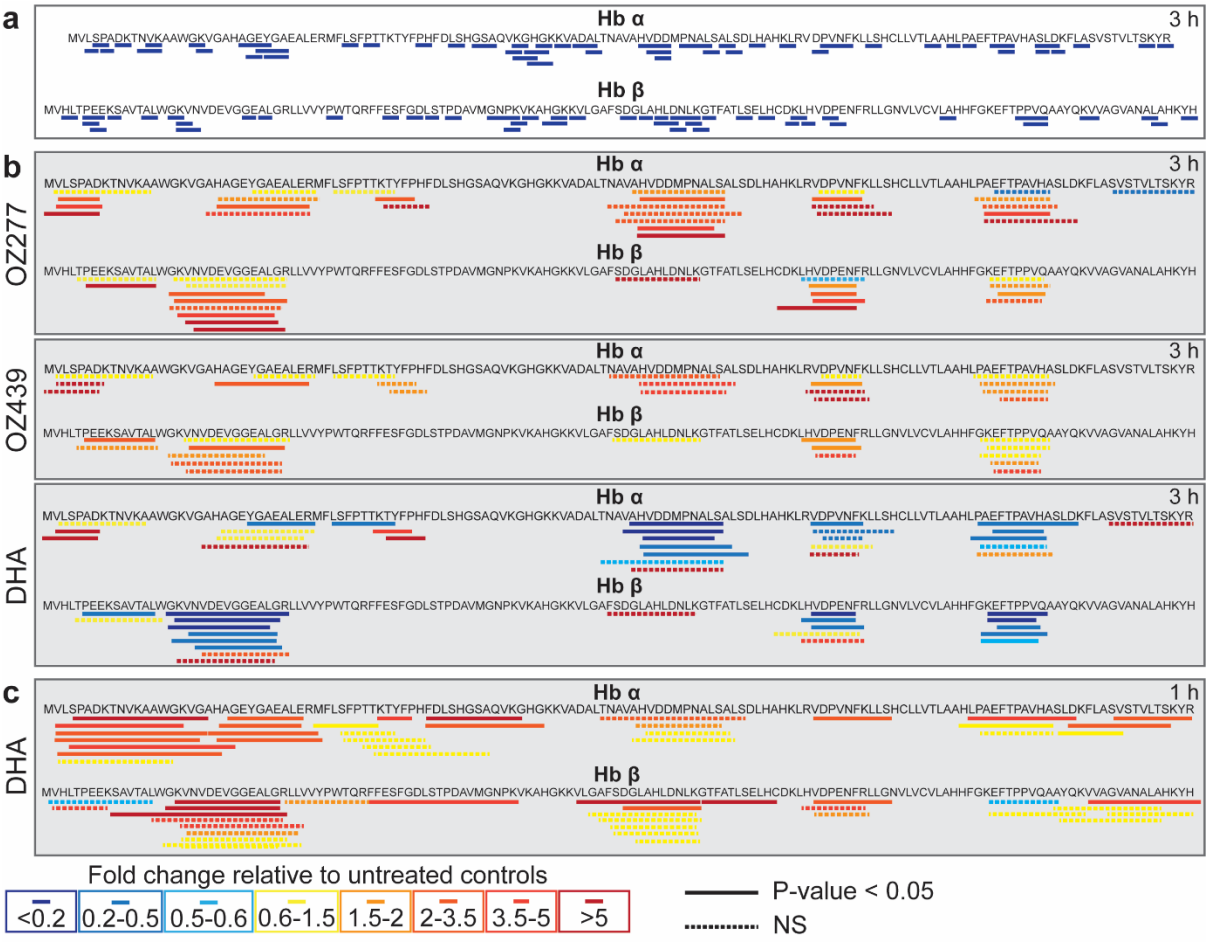

810

811

812 **Fig. 4**

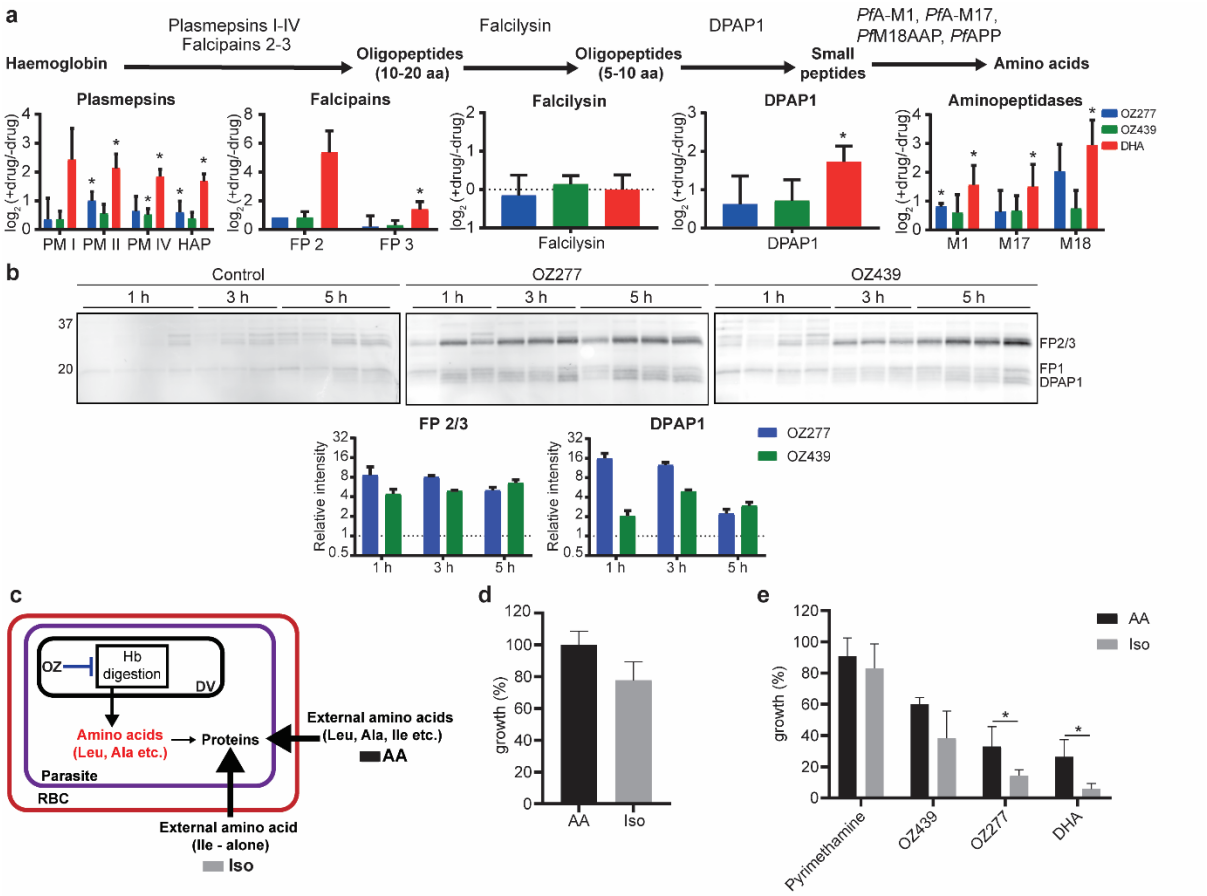

813

814

Fig. 5

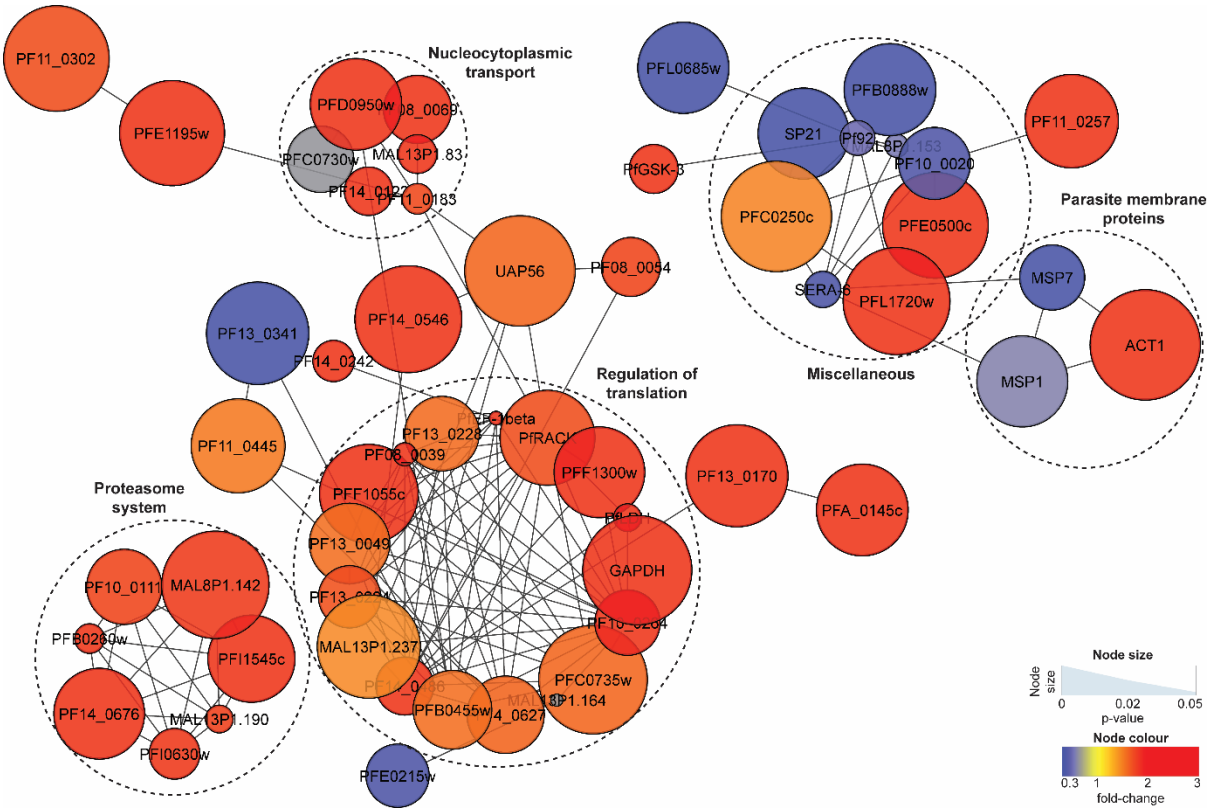

Fig. 6

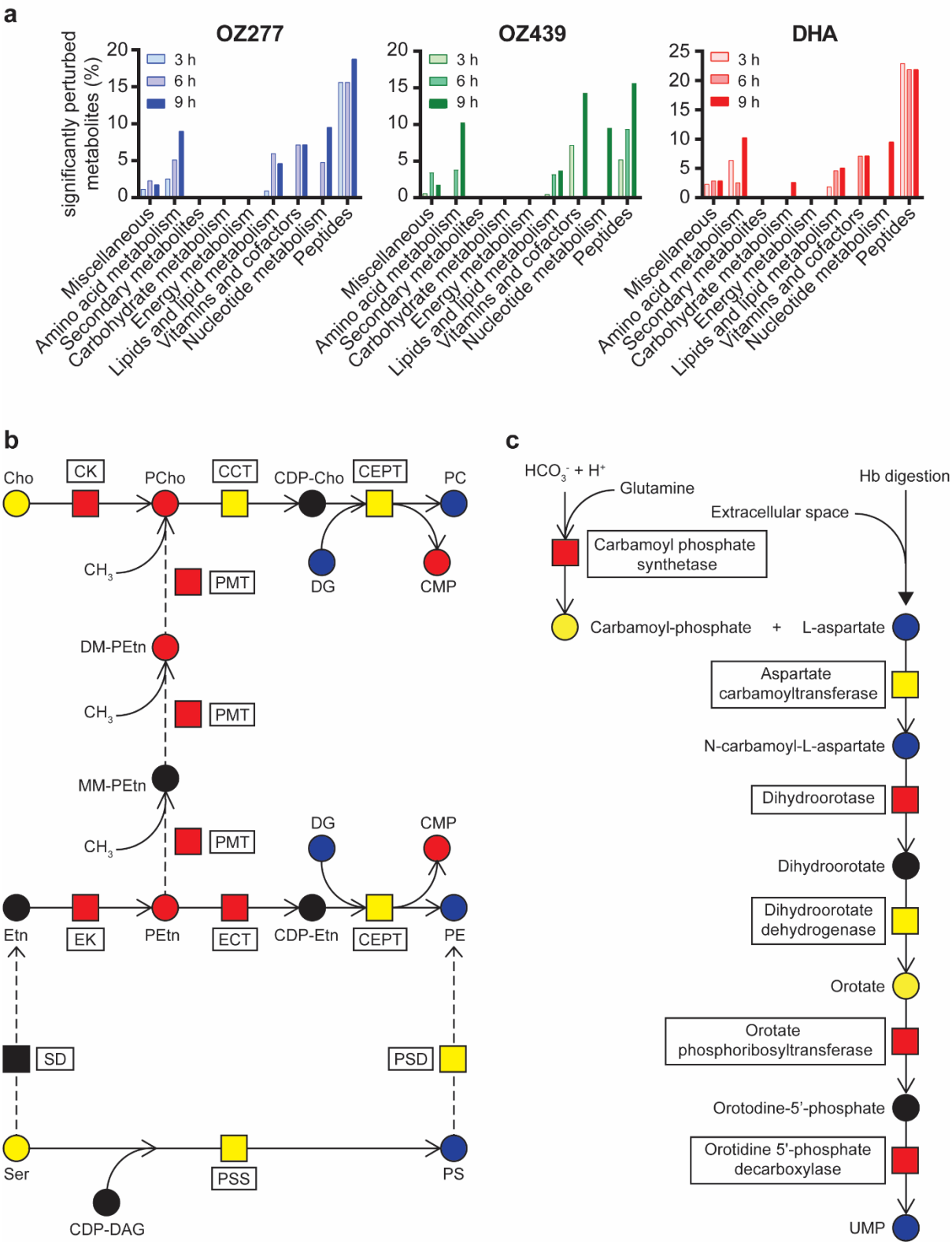

821 **Fig. 7**

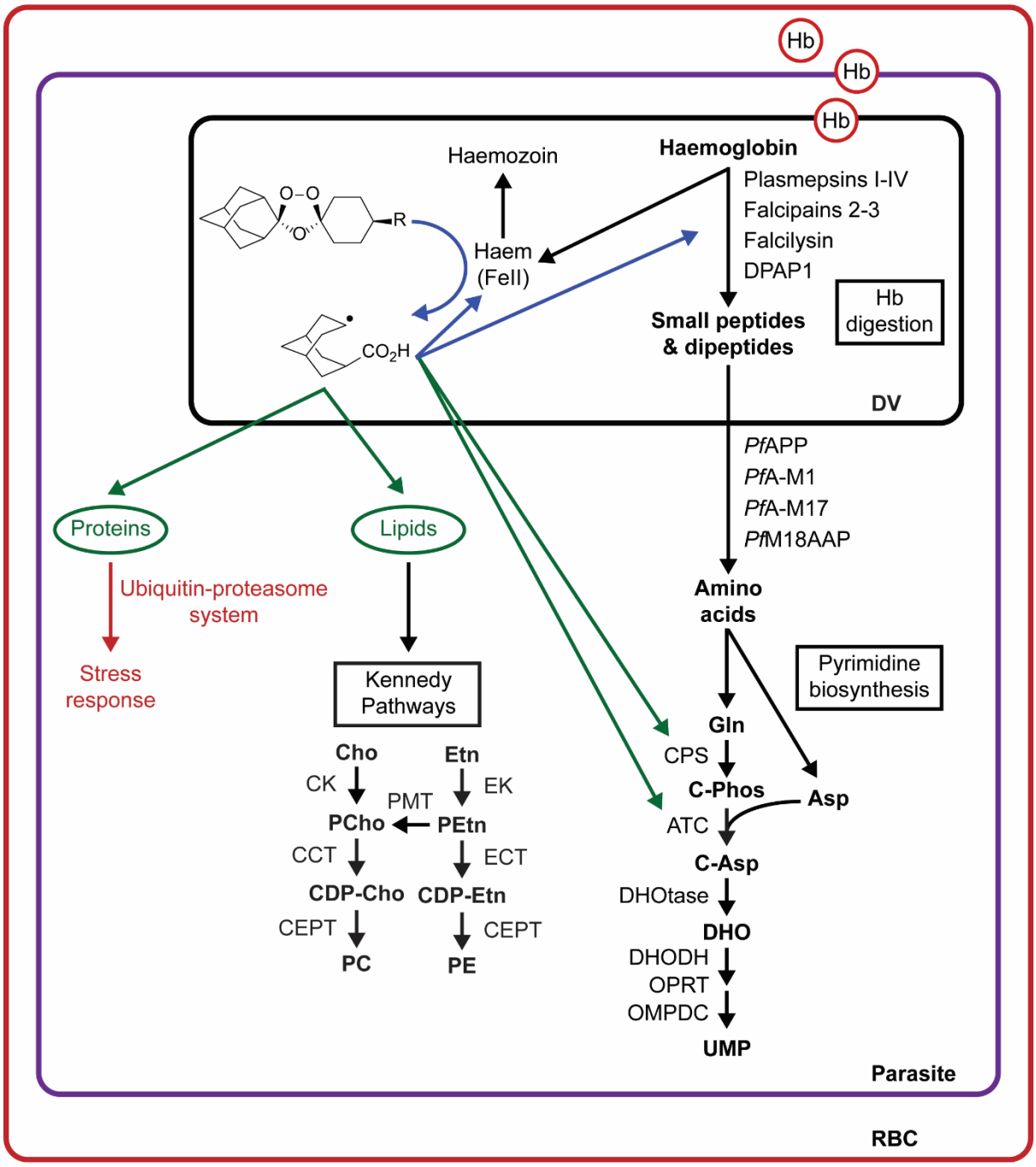

822

823

824

825 **References**

826 1. WHO. World Malaria Report 2017. Geneva: World Health Organisation, 2017.

827 2. Enserink M. Malaria's drug miracle in danger. Science. 2010; 328: 844-6. doi:
828 10.1126/science.328.5980.844. PMID: 20466917.

829 3. Meshnick SR, Thomas A, Ranz A, Xu CM, Pan HZ. Artemisinin (qinghaosu): the role
830 of intracellular hemin in its mechanism of antimalarial action. Mol Biochem Parasitol. 1991;
831 49: 181-9. doi: 10.1016/0166-6851(91)90062-B. PMID: 1775162.

832 4. Meshnick SR, Yang YZ, Lima V, Kuypers F, Kamchonwongpaisan S, Yuthavong Y.
833 Iron-dependent free radical generation from the antimalarial agent artemisinin (qinghaosu).
834 Antimicrob Agents Chemother. 1993; 37: 1108-14. doi: 10.1128/aac.37.5.1108. PMID:
835 8517699.

836 5. Posner GH, Oh CH. Regiospecifically oxygen-18 labeled 1, 2, 4-trioxane: a simple
837 chemical model system to probe the mechanism (s) for the antimalarial activity of artemisinin
838 (qinghaosu). J Am Chem Soc. 1992; 114: 8328-9. doi: 10.1021/ja00047a076.

839 6. Zhang F, Gosser DK, Meshnick SR. Hemin-catalyzed decomposition of artemisinin
840 (qinghaosu). Biochem Pharmacol. 1992; 43: 1805-9. doi: 10.1016/0006-2952(92)90713-S.
841 PMID: 1575774.

842 7. Woodrow CJ, Haynes RK, Krishna S. Artemisinins. Postgrad Med J. 2005; 81: 71-8.
843 doi: 10.1136/pgmj.2004.028399. PMID: 15701735; PubMed Central PMCID: PMC1743191.

844 8. Watsierah CA, Ouma C. Access to artemisinin-based combination therapy (ACT) and
845 quinine in malaria holoendemic regions of western Kenya. Malar J. 2014; 13: 290. doi:
846 10.1186/1475-2875-13-290. PMID: 25066600.

847 9. Wells TNC, van Huijsduijnen RH, Van Voorhis WC. Malaria medicines: a glass half
848 full? Nat Rev Drug Discov. 2015; 14: 424-42. doi: 10.1038/nrd4573.

849 10. Dondorp AM, Nosten F, Yi P, Das D, Phyo AP, Tarning J, et al. Artemisinin resistance
850 in *Plasmodium falciparum* malaria. N Engl J Med. 2009; 361: 455-67. doi:
851 10.1056/NEJMoa0808859. PMID: 19641202; PubMed Central PMCID: PMC3495232.
852 11. Vennerstrom JL, Arbe-Barnes S, Brun R, Charman SA, Chiu FC, Chollet J, et al.
853 Identification of an antimalarial synthetic trioxolane drug development candidate. Nature.
854 2004; 430: 900-4. doi: 10.1038/nature02779. PMID: 15318224.
855 12. Gautam A, Ahmed T, Sharma P, Varshney B, Kothari M, Saha N, et al.
856 Pharmacokinetics and pharmacodynamics of arterolane maleate following multiple oral doses
857 in adult patients with *P. falciparum* malaria. J Clin Pharmacol. 2011; 51: 1519-28. doi:
858 10.1177/0091270010385578. PMID: 21148048.
859 13. Saha N, Moehrle JJ, Zutshi A, Sharma P, Kaur P, Iyer SS. Safety, tolerability and
860 pharmacokinetic profile of single and multiple oral doses of arterolane (RBx11160) maleate in
861 healthy subjects. J Clin Pharmacol. 2014; 54: 386-93. doi: 10.1002/jcph.232. PMID: 24242999.
862 14. Zhou L, Alker A, Ruf A, Wang X, Chiu FC, Morizzi J, et al. Characterization of the
863 two major CYP450 metabolites of ozonide (1, 2, 4-trioxolane) OZ277. Bioorg Med Chem Lett.
864 2008; 18: 1555-8.
865 15. Charman SA, Arbe-Barnes S, Bathurst IC, Brun R, Campbell M, Charman WN, et al.
866 Synthetic ozonide drug candidate OZ439 offers new hope for a single-dose cure of
867 uncomplicated malaria. Proc Natl Acad Sci U S A. 2011; 108: 4400-5. Epub 2011/02/09. doi:
868 10.1073/pnas.1015762108. PMID: 21300861.
869 16. Moehrle JJ, Duparc S, Siethoff C, van Giersbergen PL, Craft JC, Arbe-Barnes S, et al.
870 First-in-man safety and pharmacokinetics of synthetic ozonide OZ439 demonstrates an
871 improved exposure profile relative to other peroxide antimalarials. Br J Clin Pharmacol. 2013;
872 75: 524-37. doi: 10.1111/j.1365-2125.2012.04368.x. PMID: 22759078.

17. Phyo AP, Jittamala P, Nosten FH, Pukrittayakamee S, Imwong M, White NJ, et al. Antimalarial activity of artefenomel (OZ439), a novel synthetic antimalarial endoperoxide, in patients with *Plasmodium falciparum* and *Plasmodium vivax* malaria: an open-label phase 2 trial. Lancet Infect Dis. 2016; 16: 61-9. doi: 10.1016/S1473-3099(15)00320-5. PMID: 26448141.

18. McCarthy JS, Baker M, O'Rourke P, Marquart L, Griffin P, van Huijsduijnen RH, et al. Efficacy of OZ439 (artefenomel) against early *Plasmodium falciparum* blood-stage malaria infection in healthy volunteers. J Antimicrob Chemother. 2016; 71: 2620-7. doi: 10.1093/jac/dkw174. PMID: 27272721.

19. Wang J, Zhang C-J, Chia WN, Loh CC, Li Z, Lee YM, et al. Haem-activated promiscuous targeting of artemisinin in *Plasmodium falciparum*. Nat Commun. 2015; 6: 10111.

20. Ismail HM, Barton V, Phanchana M, Charoensutthivarakul S, Wong MHL, Hemingway J, et al. Artemisinin activity-based probes identify multiple molecular targets within the asexual stage of the malaria parasites *Plasmodium falciparum* 3D7. Proc Natl Acad Sci U S A. 2016; 113: 2080-5. doi: 10.1073/pnas.1600459113. PMID: 26858419.

21. Bridgford JL, Xie SC, Cobbold SA, Pasaje CFA, Herrmann S, Yang T, et al. Artemisinin kills malaria parasites by damaging proteins and inhibiting the proteasome. Nat Commun. 2018; 9: 3801. doi: 10.1038/s41467-018-06221-1. PMID: 30228310.

22. Tilley L, Straimer J, Gnädig NF, Ralph SA, Fidock DA. Artemisinin action and resistance in *Plasmodium falciparum*. Trends Parasitol. 2016; 32: 682-96. doi: 10.1016/j.pt.2016.05.010. PMID: 27289273.

23. Bhattacharjee S, Coppens I, Mbengue A, Suresh N, Ghorbal M, Slouka Z, et al. Remodeling of the malaria parasite and host human red cell by vesicle amplification that

induces artemisinin resistance. Blood. 2018; 131: 1234-47. doi: 10.1182/blood-2017-11-814665.

24. Mbengue A, Bhattacharjee S, Pandharkar T, Liu HN, Estiu G, Stahelin RV, et al. A molecular mechanism of artemisinin resistance in *Plasmodium falciparum* malaria. Nature. 2015; 520: 683-7. doi: 10.1038/nature14412. PMID: WOS:000353689700051.

25. Tang Y, Dong Y, Wang X, Sriraghavan K, Wood JK, Vennerstrom JL. Dispiro-1,2,4-trioxane analogues of a prototype dispiro-1,2,4-trioxolane: mechanistic comparators for artemisinin in the context of reaction pathways with iron(II). J Org Chem. 2005; 70: 5103-10. doi: 10.1021/jo050385+. PMID: 15960511.

26. Jourdan J, Matile H, Reift E, Biehlmaier O, Dong Y, Wang X, et al. Monoclonal antibodies that recognize the alkylation signature of antimalarial ozonides OZ277 (arterolane) and OZ439 (artefenomel). ACS Infect Dis. 2015; 2: 54-61.

27. Ismail HM, Barton VE, Panchana M, Charoensutthivarakul S, Biagini GA, Ward SA, et al. A click chemistry-based proteomic approach reveals that 1, 2, 4-trioxolane and artemisinin antimalarials share a common protein alkylation profile. Angewandte Chemie International Ed In English. 2016; 55: 6401-5.

28. Giannangelo C, Stingelin L, Yang T, Tilley L, Charman SA, Creek DJ. Parasite-mediated degradation of synthetic ozonide antimalarials impacts *in vitro* antimalarial activity. Antimicrob Agents Chemother. 2018; 62: e01566-17. doi: 10.1128/aac.01566-17. PMID: 29263074.

29. Valecha N, Krudsood S, Tangpukdee N, Mohanty S, Sharma S, Tyagi P, et al. Arterolane maleate plus piperaquine phosphate for treatment of uncomplicated *Plasmodium falciparum* malaria: a comparative, multicenter, randomized clinical trial. Clin Infect Dis. 2012; 55: 663-71.

921 30. Yang T, Xie SC, Cao P, Giannangelo C, McCaw J, Creek DJ, et al. Comparison of the
922 exposure time-dependence of the activities of synthetic ozonide antimalarials and
923 dihydroartemisinin against K13 wild-type and mutant *Plasmodium falciparum* strains.
924 Antimicrob Agents Chemother. 2016; 60: 4501-10. doi: 10.1128/AAC.00574-16. PMID:
925 27161632.
926 31. Straimer J, Gnadig NF, Witkowski B, Amaratunga C, Duru V, Ramadani AP, et al.
927 Drug resistance. K13-propeller mutations confer artemisinin resistance in *Plasmodium*
928 *falciparum* clinical isolates. Science. 2015; 347: 428-31. doi: 10.1126/science.1260867. PMID:
929 25502314.
930 32. Dogovski C, Xie SC, Burgio G, Bridgford J, Mok S, McCaw JM, et al. Targeting the
931 cell stress response of *Plasmodium falciparum* to overcome artemisinin resistance. PLoS Biol.
932 2015; 13: e1002132. doi: 10.1371/journal.pbio.1002132. PMID: 25901609.
933 33. Rosenthal PJ, Mckerrow JH, Leech JH. A Cysteine Proteinase of *Plasmodium-*
934 *Falciparum* Trophozoites Has the Properties of Lysosomal Cathepsin-B and Cathepsin-L. Clin
935 Res. 1988; 36: A468-A. PMID: WOS:A1988M818001281.
936 34. Sijwali PS, Rosenthal PJ. Gene disruption confirms a critical role for the cysteine
937 protease falcipain-2 in hemoglobin hydrolysis by *Plasmodium falciparum*. Proc Natl Acad Sci
938 U S A. 2004; 101: 4384-9. Epub 2004/04/09. doi: 10.1073/pnas.0307720101. PMID:
939 15070727; PubMed Central PMCID: PMCPMC384756.
940 35. Combrinck JM, Fong KY, Gibhard L, Smith PJ, Wright DW, Egan TJ. Optimization of
941 a multi-well colorimetric assay to determine haem species in *Plasmodium falciparum* in the
942 presence of anti-malarials. Malar J. 2015; 14: 253. Epub 2015/06/24. doi: 10.1186/s12936-015-
943 0729-9. PMID: 26099266; PubMed Central PMCID: PMCPMC4484700.
944 36. Combrinck JM, Mabotha TE, Ncokazi KK, Ambele MA, Taylor D, Smith PJ, et al.
945 Insights into the role of heme in the mechanism of action of antimalarials. ACS Chem Biol.

946 2013; 8: 133-7. Epub 2012/10/10. doi: 10.1021/cb300454t. PMID: 23043646; PubMed Central
947 PMCID: PMCPMC3548943.
948 37. Goldberg DE. Hemoglobin degradation. In: Compans RW, Cooper MD, Honjo T,
949 Koprowski H, Melchers F, Oldstone MBA, et al., editors. Malaria: Drugs, disease and post-
950 genomic biology. Current Topics in Microbiology and Immunology. 295: Springer Berlin
951 Heidelberg; 2005. p. 275-91.
952 38. Siddiqui G, Srivastava A, Russell AS, Creek DJ. Multi-omics based identification of
953 specific biochemical changes associated with PfKelch13-mutant artemisinin resistant
954 *Plasmodium falciparum*. J Infect Dis. 2017; 215: 1435-44. Epub 2017/04/04. doi:
955 10.1093/infdis/jix156. PMID: 28368494.
956 39. Klemba M, Gluzman I, Goldberg DE. A *Plasmodium falciparum* dipeptidyl
957 aminopeptidase I participates in vacuolar hemoglobin degradation. J Biol Chem. 2004; 279:
958 43000-7. doi: 10.1074/jbc.M408123200. PMID: 15304495.
959 40. McGowan S. Working in concert: the metalloaminopeptidases from *Plasmodium*
960 *falciparum*. Curr Opin Struct Biol. 2013; 23: 828-35. doi: 10.1016/j.sbi.2013.07.015. PMID:
961 23948130.
962 41. Sanman LE, Bogyo M. Activity-based profiling of proteases. Annu Rev Biochem.
963 2014; 83: 249-73. doi: 10.1146/annurev-biochem-060713-035352. PMID: 24905783.
964 42. Greenbaum DC, Baruch A, Grainger M, Bozdech Z, Medzihradszky KF, Engel J, et al.
965 A role for the protease falcipain 1 in host cell invasion by the human malaria parasite. Science.
966 2002; 298: 2002-6. doi: 10.1126/science.1077426. PMID: 12471262.
967 43. Deu E, Leyva MJ, Albrow VE, Rice MJ, Ellman JA, Bogyo M. Functional studies of
968 *Plasmodium falciparum* dipeptidyl aminopeptidase I using small molecule inhibitors and active
969 site probes. Chem Biol. 2010; 17: 808-19. doi: 10.1016/j.chembiol.2010.06.007. PMID:
970 20797610.

971 44. Liu J, Istvan ES, Gluzman IY, Gross J, Goldberg DE. *Plasmodium falciparum* ensures
972 its amino acid supply with multiple acquisition pathways and redundant proteolytic enzyme
973 systems. Proc Natl Acad Sci U S A. 2006; 103: 8840-5. doi: 10.1073/pnas.0601876103. PMID:
974 16731623; PubMed Central PMCID: PMC1470969.
975 45. Olliaro P. Mode of action and mechanisms of resistance for antimalarial drugs.
976 Pharmacol Ther. 2001; 89: 207-19. PMID: 11316521.
977 46. Cobbold SA, Chua HH, Nijagal B, Creek DJ, Ralph SA, McConville MJ. Metabolic
978 dysregulation induced in *Plasmodium falciparum* by dihydroartemisinin and other front line
979 antimalarial drugs. J Infect Dis. 2015; 213: 276-86. doi: 10.1093/infdis/jiv372. PMID:
980 26150544.
981 47. Creek DJ, Chua HH, Cobbold SA, Nijagal B, MacRae JI, Dickerman BK, et al.
982 Metabolomics-based screening of the malaria box reveals both novel and established
983 mechanisms of action. Antimicrob Agents Chemother. 2016; 60: 6650-63. doi:
984 10.1128/aac.01226-16. PMID: 27572396.
985 48. Allman EL, Painter HJ, Samra J, Carrasquilla M, Llinás M. Metabolomic profiling of
986 the malaria box reveals antimalarial target pathways. Antimicrob Agents Chemother. 2016; 60:
987 6635-49. doi: 10.1128/AAC.01224-16. PMID: 27572391.
988 49. Sherman IW, Tanigoshi L. Incorporation of 14 C-amino-acids by malaria (*Plasmodium*
989 *lophurae*) IV. *In vivo* utilization of host cell haemoglobin. Int J Biochem. 1970; 1: 635-7. doi:
990 10.1016/0020-711X(70)90033-9.
991 50. Lew VL, Tiffert T, Ginsburg H. Excess hemoglobin digestion and the osmotic stability
992 of *Plasmodium falciparum*–infected red blood cells. Blood. 2003; 101: 4189-94. doi:
993 10.1182/blood-2002-08-2654. PMID: 12531811.
994 51. Krugliak M, Zhang J, Ginsburg H. Intraerythrocytic *Plasmodium falciparum* utilizes
995 only a fraction of the amino acids derived from the digestion of host cell cytosol for the

biosynthesis of its proteins. Mol Biochem Parasitol. 2002; 119: 249-56. doi: 10.1016/S0166-6851(01)00427-3. PMID: 11814576.

52. Francis SE, Sullivan Jr DJ, Goldberg, E D. Hemoglobin metabolism in the malaria parasite *Plasmodium falciparum*. Annu Rev Microbiol. 1997; 51: 97-123. doi: 10.1146/annurev.micro.51.1.97. PMID: 9343345.

53. Klonis N, Crespo-Ortiz MP, Bottova I, Abu-Bakar N, Kenny S, Rosenthal PJ, et al. Artemisinin activity against *Plasmodium falciparum* requires hemoglobin uptake and digestion. Proc Natl Acad Sci U S A. 2011; 108: 11405-10. doi: 10.1073/pnas.1104063108. PMID: 21709259.

54. Gruring C, Spielmann T. Imaging of live malaria blood stage parasites. Methods Enzymol. 2012; 506: 81-92. doi: 10.1016/B978-0-12-391856-7.00029-9. PMID: 22341220.

55. Orjih AU, Fitch CD. Hemozoin production by *Plasmodium falciparum*: variation with strain and exposure to chloroquine. Biochim Biophys Acta Gen Subj. 1993; 1157: 270-4. PMID: 8323956.

56. Abu Bakar N, Klonis N, Hanssen E, Chan C, Tilley L. Digestive-vacuole genesis and endocytic processes in the early intraerythrocytic stages of *Plasmodium falciparum*. J Cell Sci. 2010; 123: 441-50. Epub 2010/01/14. doi: 10.1242/jcs.061499. PMID: 20067995.

57. Straimer J, Gnädig NF, Stokes BH, Ehrenberger M, Crane AA, Fidock DA. *Plasmodium falciparum* K13 mutations differentially impact ozonide susceptibility and parasite fitness *in vitro*. mBio. 2017; 8: e00172-17. doi: 10.1128/mBio.00172-17. PMID: 28400526.

58. Rocamora F, Zhu L, Liong KY, Dondorp A, Miotto O, Mok S, et al. Oxidative stress and protein damage responses mediate artemisinin resistance in malaria parasites. PLoS Pathog. 2018; 14: e1006930. doi: 10.1371/journal.ppat.1006930. PMID: 29538461.

1020 59. Phompradit P, Chaijaroenkul W, Na-Bangchang K. Cellular mechanisms of action and
1021 resistance of *Plasmodium falciparum* to artemisinin. Parasitol Res. 2017; 116: 3331-9. doi:
1022 10.1007/s00436-017-5647-z. PMID: 29127525.
1023 60. Ponpuak M, Klemba M, Park M, Gluzman IY, Lamppa GK, Goldberg DE. A role for
1024 falcilysin in transit peptide degradation in the *Plasmodium falciparum* apicoplast. Mol
1025 Microbiol. 2007; 63: 314-34. doi: 10.1111/j.1365-2958.2006.05443.x. PMID: 17074076.
1026 61. Murata CE, Goldberg DE. *Plasmodium falciparum* falcilysin: a metalloprotease with
1027 dual specificity. J Biol Chem. 2003; 278: 38022-8. doi: 10.1074/jbc.M306842200. PMID:
1028 12876284.
1029 62. Ismail HM, Barton VE, Panchana M, Charoensutthivarakul S, Biagini GA, Ward SA,
1030 et al. A click chemistry-based proteomic approach reveals that 1, 2, 4-trioxolane and
1031 artemisinin antimalarials share a common protein alkylation profile. Angew Chem, Int Ed.
1032 2016; 55: 6401-5. doi: 10.1002/anie.201512062. PMID: 27089538.
1033 63. Wang J, Zhang C-J, Chia WN, Loh CC, Li Z, Lee YM, et al. Haem-activated
1034 promiscuous targeting of artemisinin in *Plasmodium falciparum*. Nat Commun. 2015; 6:
1035 10111. doi: 10.1038/ncomms10111. PMID: 26694030.
1036 64. Giannangelo C, Fowkes FJI, Simpson JA, Charman SA, Creek DJ. Ozonide
1037 antimalarial activity in the context of artemisinin-resistant malaria. Trends Parasitol. 2019. doi:
1038 10.1016/j.pt.2019.05.002.
1039 65. Yang T, Yeoh LM, Tutor MV, Dixon MW, McMillan PJ, Xie SC, et al. Decreased K13
1040 abundance reduces hemoglobin catabolism and proteotoxic stress, underpinning artemisinin
1041 resistance. Cell Reports. 2019; 29: 2917-28.e5. doi:
1042 https://doi.org/10.1016/j.celrep.2019.10.095.

1043 66. Birnbaum J, Scharf S, Schmidt S, Jonscher E, Hoeijmakers WAM, Flemming S, et al.
1044 A Kelch13-defined endocytosis pathway mediates artemisinin resistance in malaria parasites.
1045 Science. 2020; 367: 51-9. Epub 2020/01/04. doi: 10.1126/science.aax4735. PMID: 31896710.
1046 67. del Pilar Crespo M, Avery TD, Hanssen E, Fox E, Robinson TV, Valente P, et al.
1047 Artemisinin and a series of novel endoperoxide antimalarials exert early effects on digestive
1048 vacuole morphology. Antimicrob Agents Chemother. 2008; 52: 98-109. doi:
1049 10.1128/AAC.00609-07. PMID: 17938190.
1050 68. Maeno Y, Toyoshima T, Fujioka H, Ito Y, Meshnick SR, Benakis A, et al. Morphologic
1051 effects of artemisinin in *Plasmodium falciparum*. Am J Trop Med Hyg. 1993; 49: 485-91. Epub
1052 1993/10/01. doi: 10.4269/ajtmh.1993.49.485. PMID: 8214279.
1053 69. O'Neill PM, Posner GH. A medicinal chemistry perspective on artemisinin and related
1054 endoperoxides. J Med Chem. 2004; 47: 2945-64. doi: 10.1021/jm030571c. PMID: 15163175.
1055 70. Hartwig CL, Lauterwasser EMW, Mahajan SS, Hoke JM, Cooper RA, Renslo AR.
1056 Investigating the antimalarial action of 1,2,4-trioxolanes with fluorescent chemical probes. J
1057 Med Chem. 2011; 54: 8207-13. doi: 10.1021/jm2012003. PMID: 22023506.
1058 71. Hartwig CL, Rosenthal AS, D'Angelo J, Griffin CE, Posner GH, Cooper RA.
1059 Accumulation of artemisinin trioxane derivatives within neutral lipids of *Plasmodium*
1060 *falciparum* malaria parasites is endoperoxide-dependent. Biochem Pharmacol. 2009; 77: 322-
1061 36. doi: 10.1016/j.bcp.2008.10.015. PMID: 19022224.
1062 72. Berman PA, Adams PA. Artemisinin enhances heme-catalysed oxidation of lipid
1063 membranes. Free Radical Biol Med. 1997; 22: 1283-8. doi: 10.1016/S0891-5849(96)00508-4.
1064 PMID: 9098103.
1065 73. Serran-Aguilera L, Denton H, Rubio-Ruiz B, Lopez-Gutierrez B, Entrena A, Izquierdo
1066 L, et al. *Plasmodium falciparum* Choline Kinase Inhibition Leads to a Major Decrease in

Phosphatidylethanolamine Causing Parasite Death. Sci Rep. 2016; 6: 33189. Epub 2016/09/13. doi: 10.1038/srep33189. PMID: 27616047; PubMed Central PMCID: PMCPMC5018819.

74. Gulati S, Ekland EH, Ruggles KV, Chan RB, Jayabalasingham B, Zhou B, et al. Profiling the essential nature of lipid metabolism in asexual blood and gametocyte stages of *Plasmodium falciparum*. Cell Host Microbe. 2015; 18: 371-81. doi: 10.1016/j.chom.2015.08.003. PMID: 26355219.

75. Vielemeyer O, McIntosh MT, Joiner KA, Coppens I. Neutral lipid synthesis and storage in the intraerythrocytic stages of *Plasmodium falciparum*. Mol Biochem Parasitol. 2004; 135: 197-209. doi: 10.1016/j.molbiopara.2003.08.017. PMID: 15110461.

76. Hoang AN, Sandlin RD, Omar A, Egan TJ, Wright DW. The neutral lipid composition present in the digestive vacuole of *Plasmodium falciparum* concentrates heme and mediates β-hematin formation with an unusually low activation energy. Biochemistry. 2010; 49: 10107-16. doi: 10.1021/bi101397u. PMID: 20979358.

77. Jackson KE, Klonis N, Ferguson DJ, Adisa A, Dogovski C, Tilley L. Food vacuole-associated lipid bodies and heterogeneous lipid environments in the malaria parasite, *Plasmodium falciparum*. Mol Microbiol. 2004; 54: 109-22. doi: 10.1111/j.1365-2958.2004.04284.x. PMID: 15458409.

78. Pisciotta JM, Coppens I, Tripathi AK, Scholl PF, Shuman J, Bajad S, et al. The role of neutral lipid nanospheres in *Plasmodium falciparum* haem crystallization. Biochem J. 2007; 402: 197-204. doi: 10.1042/BJ20060986. PMID: 17044814; PubMed Central PMCID: PMC1783988.

79. Fry M, Pudney M. Site of action of the antimalarial hydroxynaphthoquinone, 2-[*trans*-4-(4'-chlorophenyl) cyclohexyl]-3-hydroxy-1,4-naphthoquinone (566C80). Biochem Pharmacol. 1992; 43: 1545-53. PMID: 1314606.

1091 80. Birrell GW, Challis MP, De Paoli A, Anderson D, Devine SM, Heffernan GD, et al.
1092 Multi-omic characterisation of the mode of action of a potent new antimalarial compound, JPC-
1093 3210, against *Plasmodium falciparum*. Mol Cell Proteomics. 2019. Epub 2019/12/15. doi:
1094 10.1074/mcp.RA119.001797. PMID: 31836637.
1095 81. Zhang M, Gallego-Delgado J, Fernandez-Arias C, Waters NC, Rodriguez A, Tsuji M,
1096 et al. Inhibiting the *Plasmodium* eIF2α kinase PK4 prevents artemisinin-induced latency. Cell
1097 Host Microbe. 2017; 22: 766-76.e4. doi: 10.1016/j.chom.2017.11.005. PMID: 29241041.
1098 82. Wek RC, Jiang H-Y, Anthony TG. Coping with stress: eIF2 kinases and translational
1099 control. Biochem Soc Trans. 2006; 34: 7-11. doi: 10.1042/bst0340007. PMID: 16246168.
1100 83. Paloque L, Ramadani AP, Mercereau-Puijalon O, Augereau J-M, Benoit-Vical F.
1101 *Plasmodium falciparum*: multifaceted resistance to artemisinins. Malar J. 2016; 15: 149. doi:
1102 10.1186/s12936-016-1206-9.
1103 84. Ponts N, Saraf A, Chung D-WD, Harris A, Prudhomme J, Washburn MP, et al.
1104 Unraveling the ubiquitome of the human malaria parasite. J Biol Chem. 2011; 286: 40320-30.
1105 doi: 10.1074/jbc.M111.238790. PMID: 21930698.
1106 85. Aminake MN, Arndt H-D, Pradel G. The proteasome of malaria parasites: A multi-
1107 stage drug target for chemotherapeutic intervention? Int J Parasitol Drugs Drug Resist. 2012;
1108 2: 1-10. doi: http://dx.doi.org/10.1016/j.ijpddr.2011.12.001.
1109 86. Macintyre F, Adoke Y, Tiono AB, Duong TT, Mombo-Ngoma G, Bouyou-Akotet M,
1110 et al. A randomised, double-blind clinical phase II trial of the efficacy, safety, tolerability and
1111 pharmacokinetics of a single dose combination treatment with artefenomel and piperaquine in
1112 adults and children with uncomplicated *Plasmodium falciparum* malaria. BMC Med. 2017; 15:
1113 181. doi: 10.1186/s12916-017-0940-3. PMID: 28988541.
1114 87. Trager W, Jensen JB. Human malaria parasites in continuous culture. Science. 1976;
1115 193: 673-5. doi: 10.1126/science.781840. PMID: 16108535.

1116 88. Lambros C, Vanderberg JP. Synchronization of *Plasmodium falciparum* erythrocytic
1117 stages in culture. J Parasitol. 1979; 65: 418-20. PMID: 383936.
1118 89. Creek DJ, Jankevics A, Burgess KE, Breitling R, Barrett MP. IDEOM: an Excel
1119 interface for analysis of LC-MS-based metabolomics data. Bioinformatics. 2012; 28: 1048-9.
1120 doi: 10.1093/bioinformatics/bts069. PMID: 22308147.
1121 90. Sumner LW, Amberg A, Barrett D, Beale MH, Beger R, Daykin CA, et al. Proposed
1122 minimum reporting standards for chemical analysis. Metabolomics. 2007; 3: 211-21. doi:
1123 10.1007/s11306-007-0082-2. PMID: 24039616.
1124 91. Creek DJ, Jankevics A, Breitling R, Watson DG, Barrett MP, Burgess KE. Toward
1125 global metabolomics analysis with hydrophilic interaction liquid chromatography-mass
1126 spectrometry: improved metabolite identification by retention time prediction. Anal Chem.
1127 2011; 83: 8703-10. doi: 10.1021/ac2021823. PMID: 21928819.
1128 92. Xia J, Sinelnikov IV, Han B, Wishart DS. MetaboAnalyst 3.0—making metabolomics
1129 more meaningful. Nucleic Acids Res. 2015; 43: W251-W7. doi: 10.1093/nar/gkv380. PMID:
1130 25897128.
1131 93. Rappsilber J, Ishihama Y, Mann M. Stop and go extraction tips for matrix-assisted laser
1132 desorption/ionization, nanoelectrospray, and LC/MS sample pretreatment in proteomics. Anal
1133 Chem. 2003; 75: 663-70. doi: 10.1021/ac026117i. PMID: 12585499
1134 94. Zhang J, Xin L, Shan B, Chen W, Xie M, Yuen D, et al. PEAKS DB: de novo
1135 sequencing assisted database search for sensitive and accurate peptide identification. Mol Cell
1136 Proteomics. 2012; 11: M111. 010587. doi: 10.1074/mcp.M111.010587. PMID: 22186715.
1137 95. Boersema PJ, Raijmakers R, Lemeer S, Mohammed S, Heck AJ. Multiplex peptide
1138 stable isotope dimethyl labeling for quantitative proteomics. Nat Protoc. 2009; 4: 484-94. doi:
1139 10.1038/nprot.2009.21. PMID: 19300442.

1140 96. Lin Y, Liu Y, Li J, Zhao Y, He Q, Han W, et al. Evaluation and optimization of removal
1141 of an acid-insoluble surfactant for shotgun analysis of membrane proteome. Electrophoresis.
1142 2010; 31: 2705-13. doi: 10.1002/elps.201000161. PMID: 20665523.
1143 97. Cox J, Mann M. MaxQuant enables high peptide identification rates, individualized
1144 ppb-range mass accuracies and proteome-wide protein quantification. Nat Biotechnol. 2008;
1145 26: 1367-72. doi: 10.1038/nbt.1511. PMID: 19029910.
1146 98. Dallas DC, Guerrero A, Parker EA, Robinson RC, Gan J, German JB, et al. Current
1147 peptidomics: Applications, purification, identification, quantification, and functional analysis.
1148 Proteomics. 2015; 15: 1026-38. doi: 10.1002/pmic.201400310. PMID: 25429922.
1149 99. Szklarczyk D, Morris JH, Cook H, Kuhn M, Wyder S, Simonovic M, et al. The
1150 STRING database in 2017: quality-controlled protein–protein association networks, made
1151 broadly accessible. Nucleic Acids Res. 2016; 45: D362-D8. doi: 10.1093/nar/gkw937. PMID:
1152 27924014.
1153 100. Shannon P, Markiel A, Ozier O, Baliga NS, Wang JT, Ramage D, et al. Cytoscape: A
1154 software environment for integrated models of biomolecular interaction networks. Genome
1155 Res. 2003; 13: 2498-504. doi: 10.1101/gr.1239303. PMID: 14597658.
1156 101. Edgington LE, Bogyo M. *In vivo* imaging and biochemical characterization of protease
1157 function using fluorescent activity-based probes. Curr Protoc Chem Biol. 2013; 5: 25-44. doi:
1158 10.1002/9780470559277.ch120235. PMID: 23788323.
1159 102. Xie SC, Dogovski C, Kenny S, Tilley L, Klonis N. Optimal assay design for
1160 determining the *in vitro* sensitivity of ring stage *Plasmodium falciparum* to artemisinins. Int J
1161 Parasitol. 2014; 44: 893-9. doi: 10.1016/j.ijpara.2014.07.008.
1162 103. Perez-Riverol Y, Csordas A, Bai J, Bernal-Llinares M, Hewapathirana S, Kundu DJ, et
1163 al. The PRIDE database and related tools and resources in 2019: improving support for
1164 quantification data. Nucleic Acids Res. 2018; 47: D442-D50. doi: 10.1093/nar/gky1106.

1165 **Supporting information**

1166 **Supplementary Dataset 1. IDEOM metabolomics output for OZ277, OZ439 and DHA**
1167 **treatment of *P. falciparum* (3D7 strain) ring and trophozoite infected RBC cultures and**
1168 **uninfected RBC cultures.**

1169 **Supplementary Dataset 2. IDEOM metabolomics output for OZ277, OZ439 and DHA**
1170 **treatment of Cam3.II^{R539T} (artemisinin resistant) and Cam3.II^{rev} (artemisinin sensitive)**
1171 ***P. falciparum* parasite lines.**

1172 **Supplementary Dataset 3. Peptidomics dataset for OZ277, OZ439 and DHA treatment (3**
1173 **h) of *P. falciparum* trophozoite infected RBC cultures (3D7 strain).**

1174 **Supplementary Dataset 4. Peptidomics dataset for DHA (1 h) treatment of *P. falciparum***
1175 **trophozoite infected RBC cultures (Cam3.II^{rev}, artemisinin sensitive).**

1176 **Supplementary Dataset 5. Proteomics dataset for OZ277, OZ439 and DHA treatment of**
1177 ***P. falciparum* trophozoite infected RBC cultures (3D7 strain).**

1178

OZ277 (arterolane)

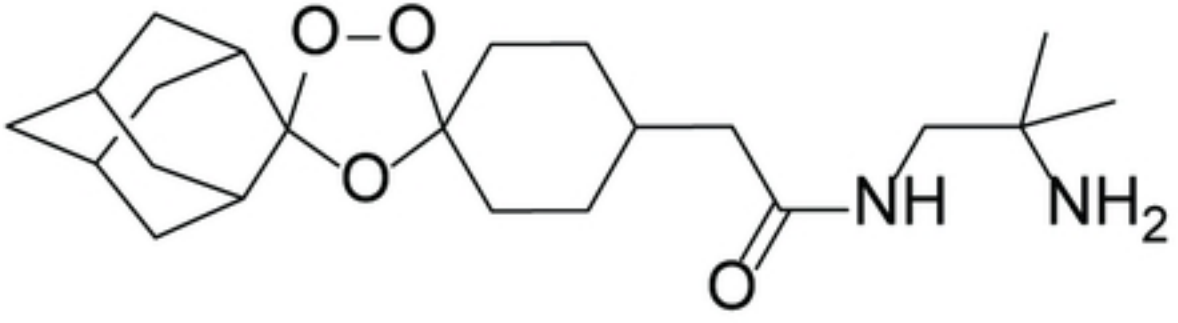

dihydroartemisinin (DHA)

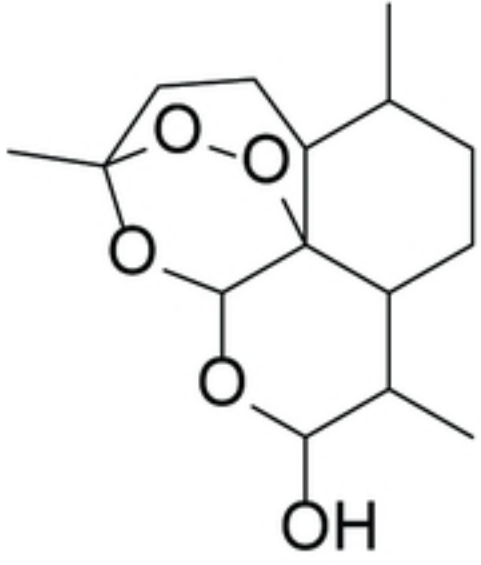

OZ439 (artefenomel)

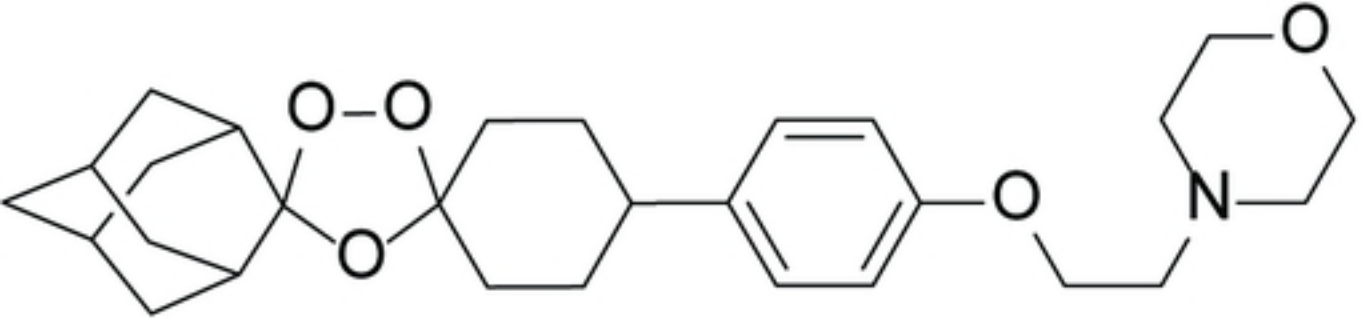

Figure 1

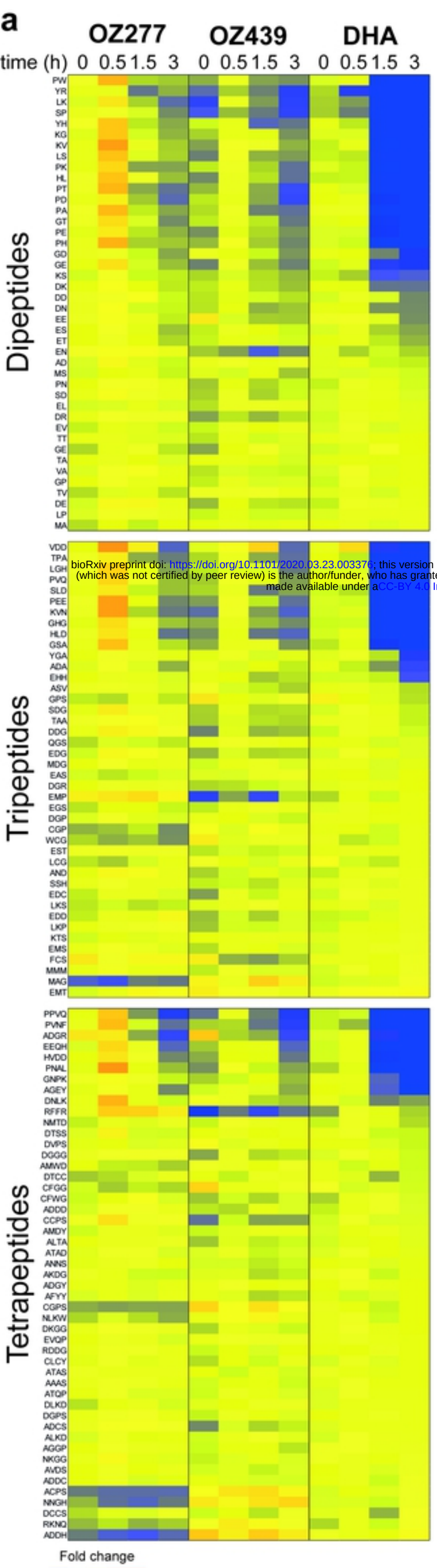

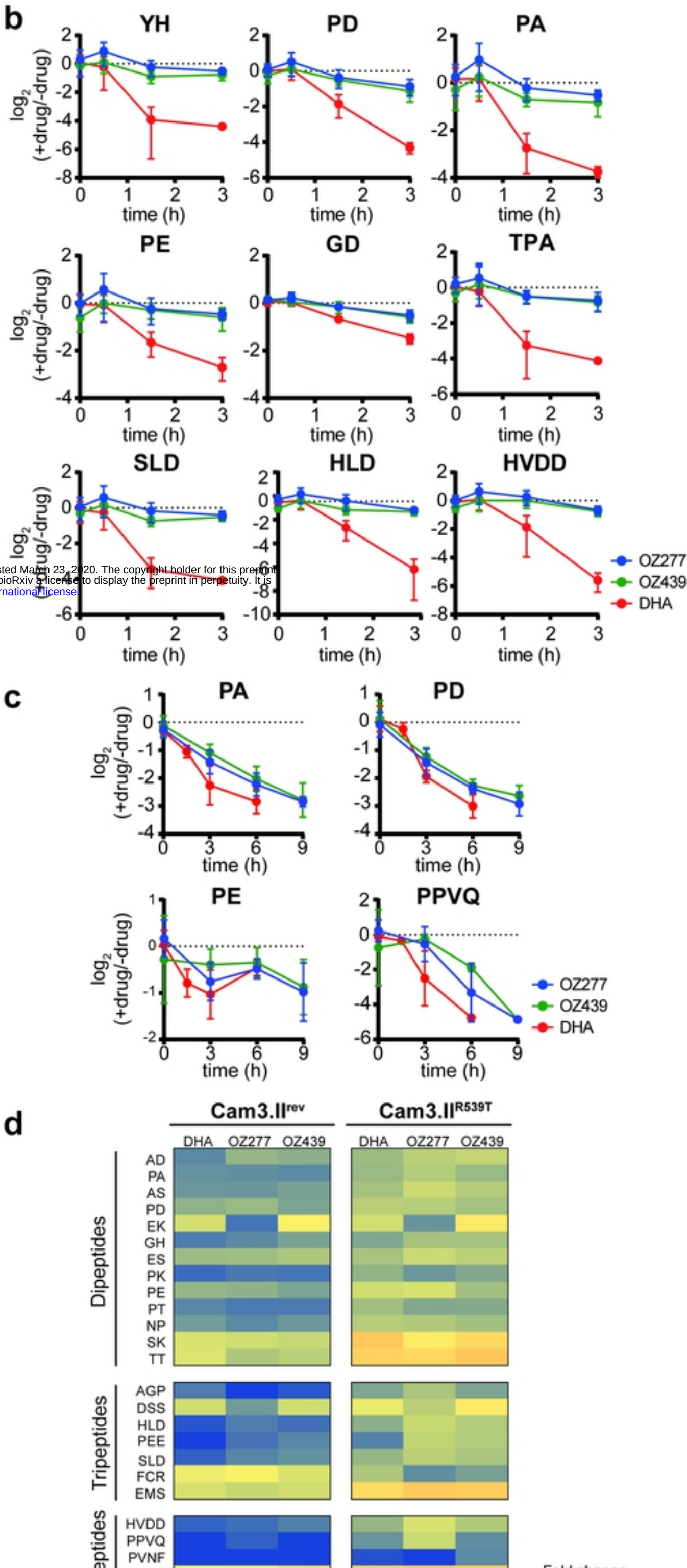

Figure 2

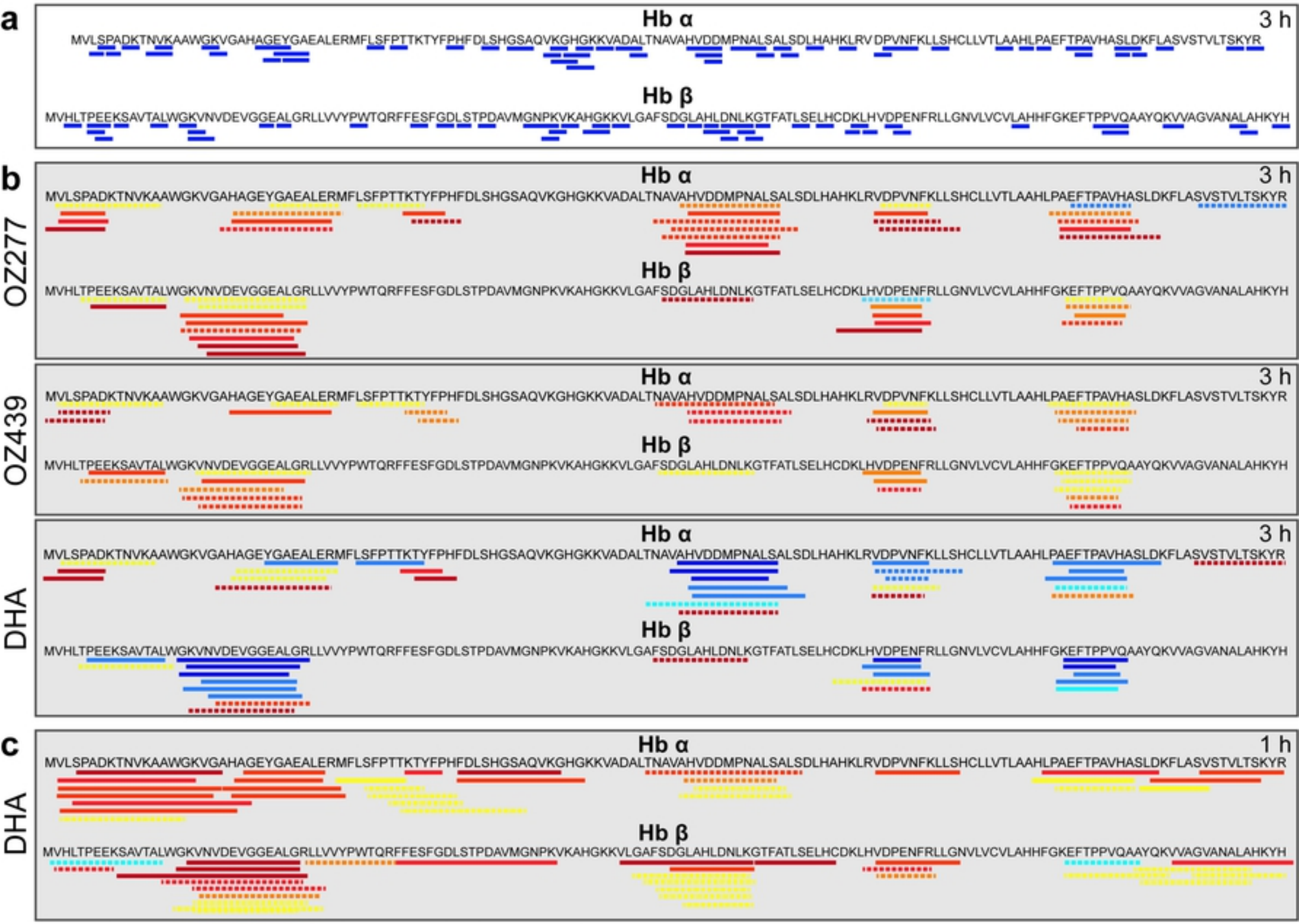
a
Hb α
3 h
MVLSPADKTNVKAAWGKVGAHAGEYGAEALERMFLSFPTTKTYFPHFDLSHGSAQVKGHGKKVADALTNAVAHVDDMPNALSALSDLHAHKLRV DPVNFKLLSHCLLVTLAAHLPAEFTPAVHASLDKFLASVSTVLTSKYR
Hb β
MVHLTPEEKSAVTALWGKVNVDEVGGEALGRLLVVYPWTQRFFESFGDLSTPDAVMGNPKVKAHGKKVLGAFSDGLAHLDNLKGTFATLSELHCDKLHVDPENFRLLGNVLVCVLAHHFGKEFTPPVQAAYQKVVAGVANALAHKYH
b
OZ277
Hb α
3 h
MVLSPADKTNVKAAWGKVGAHAGEYGAEALERMFLSFPTTKTYFPHFDLSHGSAQVKGHGKKVADALTNAVAHVDDMPNALSALSDLHAHKLRVDPVNFKLLSHCLLVTLAAHLPAEFTPAVHASLDKFLASVSTVLTSKYR
Hb β
MVHLTPEEKSAVTALWGKVNVDEVGGEALGRLLVVYPWTQRFFESFGDLSTPDAVMGNPKVKAHGKKVLGAFSDGLAHLDNLKGTFATLSELHCDKLHVDPENFRLLGNVLVCVLAHHFGKEFTPPVQAAYQKVVAGVANALAHKYH
OZ439
Hb α
3 h
MVLSPADKTNVKAAWGKVGAHAGEYGAEALERMFLSFPTTKTYFPHFDLSHGSAQVKGHGKKVADALTNAVAHVDDMPNALSALSDLHAHKLRVDPVNFKLLSHCLLVTLAAHLPAEFTPAVHASLDKFLASVSTVLTSKYR
Hb β
MVHLTPEEKSAVTALWGKVNVDEVGGEALGRLLVVYPWTQRFFESFGDLSTPDAVMGNPKVKAHGKKVLGAFSDGLAHLDNLKGTFATLSELHCDKLHVDPENFRLLGNVLVCVLAHHFGKEFTPPVQAAYQKVVAGVANALAHKYH
DHA
Hb α
3 h
MVLSPADKTNVKAAWGKVGAHAGEYGAEALERMFLSFPTTKTYFPHFDLSHGSAQVKGHGKKVADALTNAVAHVDDMPNALSALSDLHAHKLRVDPVNFKLLSHCLLVTLAAHLPAEFTPAVHASLDKFLASVSTVLTSKYR
Hb β
MVHLTPEEKSAVTALWGKVNVDEVGGEALGRLLVVYPWTQRFFESFGDLSTPDAVMGNPKVKAHGKKVLGAFSDGLAHLDNLKGTFATLSELHCDKLHVDPENFRLLGNVLVCVLAHHFGKEFTPPVQAAYQKVVAGVANALAHKYH
c
DHA
Hb α
1 h
MVLSPADKTNVKAAWGKVGAHAGEYGAEALERMFLSFPTTKTYFPHFDLSHGSAQVKGHGKKVADALTNAVAHVDDMPNALSALSDLHAHKLRVDPVNFKLLSHCLLVTLAAHLPAEFTPAVHASLDKFLASVSTVLTSKYR
Hb β
MVHLTPEEKSAVTALWGKVNVDEVGGEALGRLLVVYPWTQRFFESFGDLSTPDAVMGNPKVKAHGKKVLGAFSDGLAHLDNLKGTFATLSELHCDKLHVDPENFRLLGNVLVCVLAHHFGKEFTPPVQAAYQKVVAGVANALAHKYH
Fold change relative to untreated controls
<0.2
0.2-0.5
0.5-0.6
0.6-1.5
1.5-2
2-3.5
3.5-5
>5
P-value < 0.05
NS

Figure 3

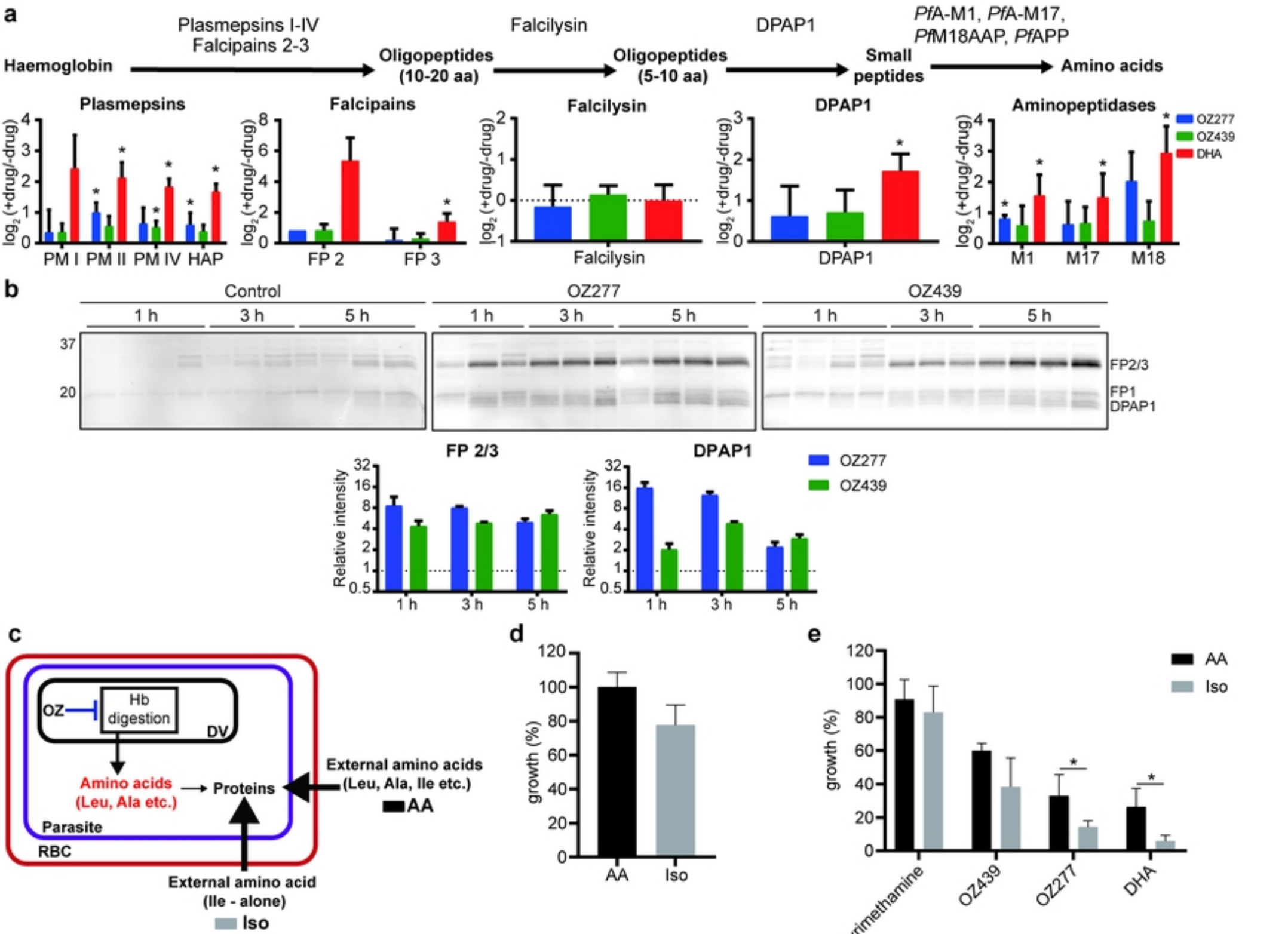
a
Plasmepsins I-IV
Falcipains 2-3
Falcilysin
DPAP1
PfA-M1, PfA-M17,
PfM18AAP, PfAPP
Haemoglobin
Oligopeptides
(10-20 aa)
Oligopeptides
(5-10 aa)
Small
peptides
Amino acids
Plasmepsins
Falcipains
Falcilysin
DPAP1
Aminopeptidases
log2 (+drug/-drug)
PM I
PM II
PM IV
HAP
FP 2
FP 3
Falcilysin
DPAP1
M1
M17
M18
OZ277
OZ439
DHA
b
Control
OZ277
OZ439
1 h
3 h
5 h
37
20
FP2/3
FP1
DPAP1
FP 2/3
DPAP1
Relative intensity
c
OZ
Hb
digestion
DV
Amino acids
(Leu, Ala etc.)
Proteins
Parasite
RBC
External amino acids
(Leu, Ala, Ile etc.)
AA
External amino acid
(Ile - alone)
Iso
d
growth (%)
AA
Iso
e
growth (%)
AA
Iso
Pyrimethamine
OZ439
OZ277
DHA

Figure 4

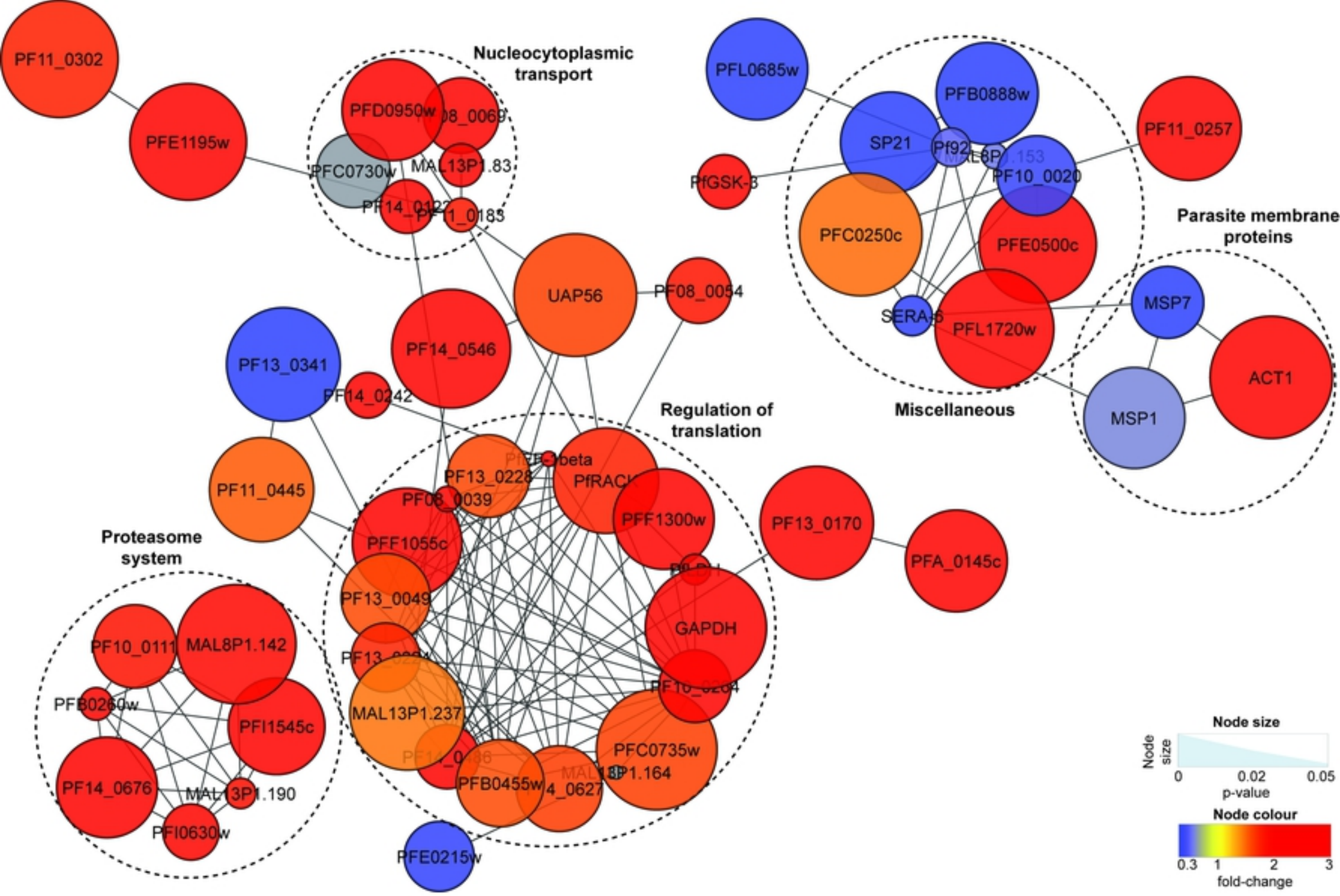
Nucleocytoplasmic transport
Regulation of translation
Proteasome system
Miscellaneous
Parasite membrane proteins
PF11_0302
PFE1195w
PFD0950w
PFC0730w
MAL13P1.83
PF14_0127
PF11_0183
PFL0685w
PFB0888w
SP21
PF92
PF10_0020
PF11_0257
PfGSK-3
PFC0250c
PFE0500c
SERA-5
PFL1720w
MSP7
ACT1
MSP1
UAP56
PF08_0054
PF14_0546
PF13_0341
PF14_0242
PF11_0445
PF13_0228
PF08_0039
PFF1300w
PF13_0170
PFA_0145c
PFF1055c
PF13_0049
GAPDH
MAL13P1.237
PFC0735w
PFB0455w
PFE0215w
PF10_0111
MAL8P1.142
PFB0260w
PFI1545c
PF14_0676
MAL13P1.190
PFI0630w
Node size
Node size
0
0.02
0.05
p-value
Node colour
0.3
1
2
3
fold-change

Figure 5

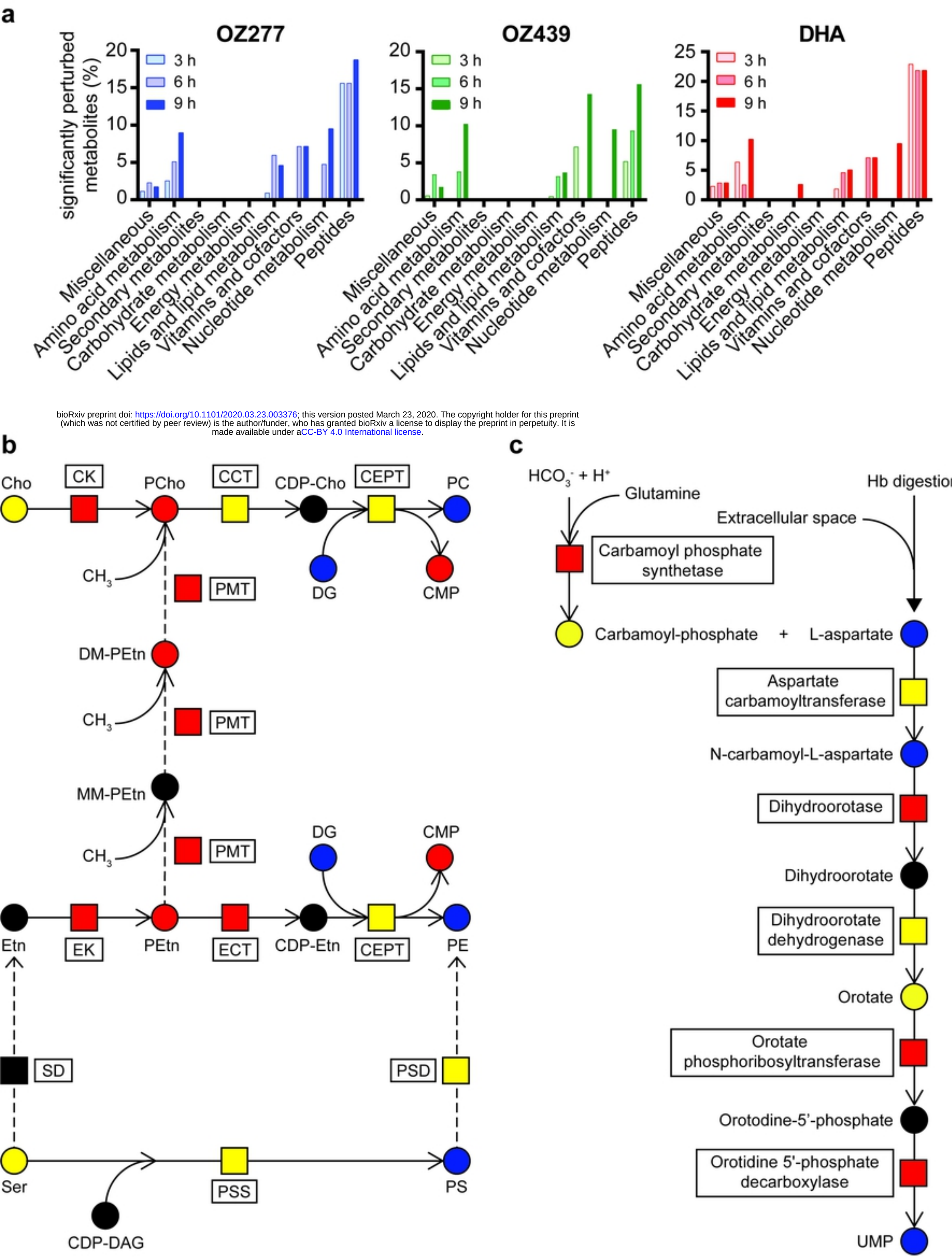

Figure 6

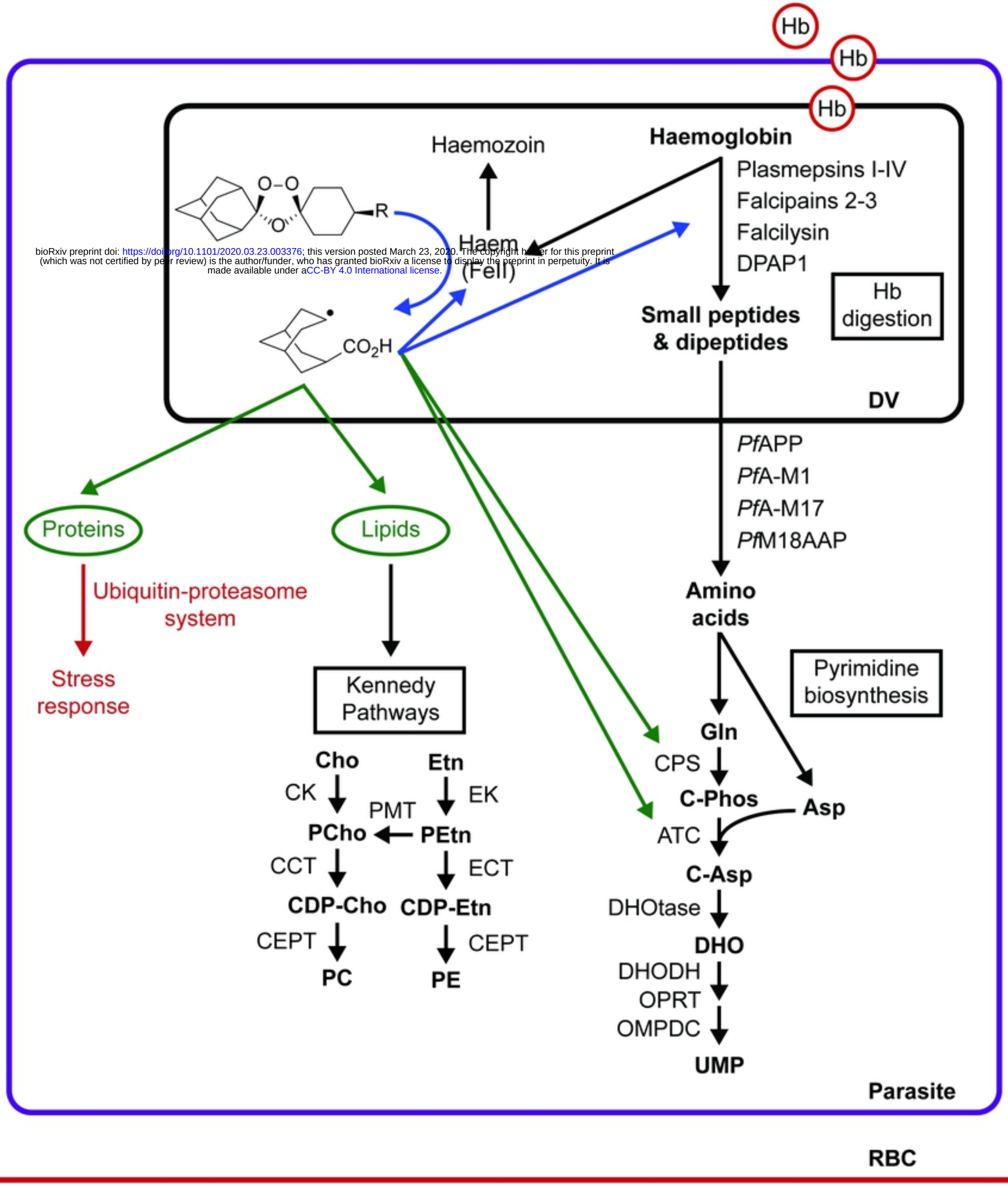

Figure 7